AD-A277 191

14

TECHNICAL REPORT

Naval Facilities Engineering Service Center, Port Hueneme, CA 93043-4328

BOND STRESS-SLIP CHARACTERISTICS OF FRP REBARS

94-08827

TR-2013-SHR

DTIC

February 1994

By L.J. Malvar

Sponsored by
Office of Naval Research

The bond characteristics of four different types of glass fiber-reinforced plastic (GFRP) rebars with different surface deformations were analyzed experimentally. Local bond stress-slip data, as well as bond stress-radial deformation data, needed for constitutive modeling of the interface mechanics, were obtained for varying levels of confining pressure. In addition to bond stress and slip, radial stress and radial deformation were considered fundamental variables needed to provide for configuration-independent relationships. Each test specimen consisted of a #6 GFRP rebar embedded in a 3-inch-diameter, 4-inch-long cracked concrete cylinder subjected to a controlled, constant amount of confining axisymmetric radial pressure. Only 2.625 inches (the equivalent of five steel bar lugs) of contact were allowed between the bar and the concrete. For each rebar type, bond stress-slip and bond stress-radial deformation relationships were obtained for five levels of confining axisymmetric radial pressure. It was found that small surface indentations are sufficient to yield bond strengths comparable to that of steel bars. Effects of the deformations on tensile properties are discussed. It is also shown that radial pressure is an important parameter which can increase the bond strength threefold.

Approved for public release; distribution unlimited.

94 3 10 4

METRIC CONVERSION FACTORS

Approximate Conversions to Metric Measures

Symbol	When You Know	Multiply by	To Find	Symbol
		LENGTH		
in	inches	*2.5	centimeters	cm
ft	feet	30	centimeters	cm
yd	yards	0.9	meters	m
mi	miles	1.6	kilometers	km
		AREA		
in^2	square inches	6.5	square centimeters	cm^2
ft^2	square feet	0.09	square meters	m^2
yd^2	square yards	0.8	square meters	m^2
mi^2	square miles	2.6	square kilometers	km^2
	acres	0.4	hectares	ha
		MASS (weight)		
oz	ounces	28	grams	g
lb	pounds	0.45	kilograms	kg
	short tons (2,000 lb)	0.9	tonnes	t
		VOLUME		
tsp	teaspoons	5	milliliters	ml
Tbsp	tablespoons	15	milliliters	ml
fl oz	fluid ounces	30	milliliters	ml
c	cups	0.24	liters	l
pt	pints	0.47	liters	l
qt	quarts	0.95	liters	l
gal	gallons	3.8	liters	l
ft^3	cubic feet	0.03	cubic meters	m^3
yd^3	cubic yards	0.76	cubic meters	m^3
		TEMPERATURE (exact)		
°F	Fahrenheit temperature	5/9 (after subtracting 32)	Celsius temperature	°C

*1 in = 2.54 (exactly). For other exact conversions and more detailed tables, see NBS Misc. Publ. 286, Units of Weights and Measures, Price $2.25, SD Catalog No. C13.10:286.

Approximate Conversions from Metric Measures

Symbol	When You Know	Multiply by	To Find	Symbol
		LENGTH		
mm	millimeters	0.04	inches	in
cm	centimeters	0.4	inches	in
m	meters	3.3	feet	ft
m	meters	1.1	yards	yd
km	kilometers	0.6	miles	mi
		AREA		
cm^2	square centimeters	0.16	square inches	in^2
m^2	square meters	1.2	square yards	yd^2
km^2	square kilometers	0.4	square miles	mi^2
ha	hectares (10,000 m^2)	2.5	acres	
		MASS (weight)		
g	grams	0.035	ounces	oz
kg	kilograms	2.2	pounds	lb
t	tonnes (1,000 kg)	1.1	short tons	
		VOLUME		
ml	milliliters	0.03	fluid ounces	fl oz
l	liters	2.1	pints	pt
l	liters	1.06	quarts	qt
l	liters	0.26	gallons	gal
m^3	cubic meters	35	cubic feet	ft^3
m^3	cubic meters	1.3	cubic yards	yd^3
		TEMPERATURE (exact)		
°C	Celsius temperature	9/5 (then add 32)	Fahrenheit temperature	°F

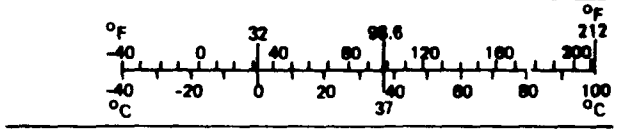

REPORT DOCUMENTATION PAGE

Form Approved
OMB No. 0704-018

Public reporting burden for this collection of information is estimated to average 1 hour per response, including the time for reviewing instructions, searching existing data sources, gathering and maintaining the data needed, and completing and reviewing the collection of information. Send comments regarding this burden estimate or any other aspect of this collection information, including suggestions for reducing this burden, to Washington Headquarters Services, Directorate for Information and Reports, 1215 Jefferson Davis Highway, Suite 1204, Arlington, VA 22202-4302, and to the Office of Management and Budget, Paperwork Reduction Project (0704-0188), Washington, DC 20503.

1. AGENCY USE ONLY *(Leave blank)*	2. REPORT DATE	3. REPORT TYPE AND DATES COVERED
	February 1994	Interim; FY92 through FY93

4. TITLE AND SUBTITLE

BOND STRESS-SLIP CHARACTERISTICS OF FRP REBARS

5. FUNDING NUMBERS

PR - YR023.03.001
WU - DN666342

6. AUTHOR(S)

L. J. Malvar

7. PERFORMING ORGANIZATION NAME(S) AND ADDRESSE(S)

Naval Facilities Engineering Service Center
560 Center Drive
Port Hueneme, CA 93043-4328

8. PERFORMING ORGANIZATION REPORT NUMBER

TR-2013-SHR

9. SPONSORING/MONITORING AGENCY NAME(S) AND ADDRESSE(S)

Office of Naval Research
Arlington, VA 22217-5000

10. SPONSORING/MONITORING AGENCY REPORT NUMBER

11. SUPPLEMENTARY NOTES

12a. DISTRIBUTION/AVAILABILITY STATEMENT

Approved for public release; distribution unlimited.

12b. DISTRIBUTION CODE

13. ABSTRACT *(Maximum 200 words)*

The bond characteristics of four different types of glass fiber-reinforced plastic (GFRP) rebars with different surface deformations were analyzed experimentally. Local bond stress-slip data, as well as bond stress-radial deformation data, needed for constitutive modeling of the interface mechanics, were obtained for varying levels of confining pressure. In addition to bond stress and slip, radial stress and radial deformation were considered fundamental variables needed to provide for configuration-independent relationships. Each test specimen consisted of a #6 GFRP rebar embedded in a 3-inch-diameter, 4-inch-long cracked concrete cylinder subjected to a controlled, constant amount of confining axisymmetric radial pressure. Only 2.625 inches (the equivalent of five steel bar lugs) of contact were allowed between the bar and the concrete. For each rebar type, bond stress-slip and bond stress-radial deformation relationships were obtained for five levels of confining axisymmetric radial pressure. It was found that small surface indentations are sufficient to yield bond strengths comparable to that of steel bars. Effects of the deformations on tensile properties are discussed. It is also shown that radial pressure is an important parameter which can increase the bond strength threefold.

14. SUBJECT TERMS

Glass fiber-reinforced plastic rebars, stress-slip data, stress-radial deformation data, modeling, confining pressure, bond strengths

15. NUMBER OF PAGES

51

16. PRICE CODE

17. SECURITY CLASSIFICATION OF REPORT	18. SECURITY CLASSIFICATION OF THIS PAGE	19. SECURITY CLASSIFICATION OF ABSTRACT	20. LIMITATION OF ABSTRACT
Unclassified	Unclassified	Unclassified	UL

PREFACE

On 1 October 1993, the Naval Civil Engineering Laboratory (NCEL) was consolidated with five other Naval Facilities Engineering Command (NAVFAC) components into the Naval Facilities Engineering Service Center (NFESC). Due to publishing timeframes, this document may have references to NCEL instead of NFESC.

Accesion For	
NTIS CRA&I	X
DTIC TAB	☐
Unannounced	☐
Justification	
By	
Distribution /	
Availability Codes	
Dist	Avail and / or Special
A-1	

CONTENTS

INTRODUCTION

Extensive and costly condition assessment, repair, and rehabilitation programs are underway to extend the service life of Navy shore facilities. The main cause of deterioration is the corrosion of the steel reinforcement exposed to the marine environment and aggressive agents such as deicing salts for bridges and pavements. To prevent this corrosion, galvanized and epoxy-coated bars are currently being used and investigated (Refs 1 through 4), with mixed results (Ref 2). A more recent alternative is the use of fiber-reinforced plastic (FRP) rebars which have excellent corrosion resistance properties and mechanical properties similar to steel (Refs 5 and 6). FRP rebars, tendons, and grating have already been extensively used in waterfront structures and bridges (Refs 6 through 11).

BACKGROUND

A main concern with FRP rebars, as well as epoxy-coated rebars, is the behavior of the interface between FRP rebars and concrete, which has not yet been satisfactorily evaluated. Bond characteristics primarily affect anchorage requirements. For FRP rebar, bond characteristics are currently being investigated by many researchers (Refs 12 through 19). The acceptance of FRP rebar in structural engineering has been inhibited due to the lack of design criteria, particularly with regard to bond (Refs 20 and 21). One reason for the lack of design criteria for bond is the lack of standards for the geometry of the bar deformations.

OBJECTIVE

The objective of this study is to develop an understanding of bond-slip behavior for currently available FRP rebars for application to the analysis and design of reinforced concrete waterfront facilities. A comparative study of various deformation geometries is also carried out, which is expected to yield information applicable to bars composed of other materials.

For each FRP rebar, bond stress-slip constitutive relationships are experimentally determined. The data are obtained as a family of bond stress-slip curves for five levels of constant radial confining stress. In addition, bond stress-radial deformation curves are obtained which characterize the radial expansion at the interface. These experimental data will be useful for mathematical or numerical modeling of structural behavior which includes bond. In turn, these models can be used to determine anchorage requirements for FRP rebars without need for extensive testing.

TENSILE AND BOND TESTS FOR FRP REBARS

Four commercially available FRP rebar types with different deformations were analyzed experimentally and their mechanical properties obtained.

Rebar Types

The four rebars considered are shown in Figure 1. Only nominal 3/4-inch-diameter bars were studied. All four are composed of pultruded E-glass fibers with an approximate fiber volume fraction of 45 percent (60 percent by weight) embedded in a vinyl ester or polyester resin matrix. For each bar, Table 1 presents the deformation spacing, in inches, and as a fraction of the nominal bar diameter ∅, which is 0.75 inches in this case. For steel bars, the maximum deformation spacing is 0.7 ∅ (i.e., 0.525 inches for a #6 bar) (Ref 22). The coefficient of variation of the measurements is reported. The clear spacing is defined as the spacing minus the deformation width. Table 1 also indicates the deformation height (or the indentation depth) in inches and as a fraction of the diameter, as well as the corresponding coefficient of variation. The deformation height (or indentation depth) is measured as the difference between the bar radius at a deformation and the radius at midpoint between that deformation and the next one.

In addition, each bar type has the following characteristics:

1. Type A - These bars have an external helicoidal tow which provides both a protruding deformation and a small indentation of the bar surface. An outer layer consisting exclusively of matrix material is provided around the fibers for additional protection. In this case, the deformation width was about 0.125 inch, yielding a clear deformation spacing of 0.595 inch.

2. Type B - During the fabrication of these bars, the surface tow is stressed so that indentations are obtained instead of deformations. These bars showed a large variation of cross section which was expected to yield a large variation in mechanical properties. In addition, the surface indentations provided to carry the bond stresses appeared very pronounced in some bars and non-existent in others. A large scatter was expected in the bond tests as well.

3. Type C - These bars have the surface tow glued to the exterior of the bar to provide only surface deformations. The fibers in the bar itself are perfectly straight.

4. Type D - Here an indentation similar to the one in type B is provided. These bars appear to have an outer veil to protect the glass fibers.

Tensile Tests

For each bar type, five tensile tests following ASTM D3916-84 (Ref 23) were first conducted to determine the secant modulus of elasticity (at 24 ksi), the ultimate stress, and the ultimate strain (series 1). Elongation measurements were taken using two LVDTs on either side of each bar, attached via two clamps spaced an average of 13 inches. Total specimen length was 42 inches with a clear spacing between grips of about 28 inches.

It was decided that these tests, which use an actual bar specimen, would be more representative than the ones under ASTM D638-90 (Ref 24), which requires a machined down specimen. The shortcomings of using a machined specimen are that the effects of indentation and specimen size on tensile strength cannot be evaluated, and the bar cross-sectional area may not be easily determined. The shortcomings of using an undisturbed bar specimen are related to grip effects. These grip effects are described in a later section.

To alleviate these grip effects, three more tensile tests were conducted for Types A and C (series 2). In these tests, specially designed grips consisting of four aluminum blocks bolted together were used. Shims consisting of strips from a 3/4-inch annealed aluminum pipe were inserted between grips and specimens. Only ultimate stresses are reported for this series.

Bond Tests

The objective of these tests was to determine configuration-independent, local bond stress-slip data for use in constitutive material models. Typically, bond stress-slip curves are derived from pullout tests, or other more complex setups, without regard for the lateral confinement exerted by the particular setup. As a result, very disparate curves have been obtained which are only representative of the particular setup. If the lateral confinement is taken into account, a family of curves can be obtained, which could be used with any other configuration. The proposed tests have already been carried out for steel bars (Refs 25 to 27) yielding general bond stress-slip relationships successfully used in predicting a variety of well known results reported in the literature (Refs 28 to 30).

The specimen used is shown in Figure 2. It consists of a 3-inch-diameter, 4-inch-long concrete cylinder surrounding an FRP rebar. Only 2.625 inches of the bar are actually in contact with the concrete, with contact being prevented in the rest of the specimen via silicone-rubber spacers. The outer concrete surface is surrounded by a split, threaded steel pipe which carries the pullout force via shear stresses (Figure 3). The pipe is split into eight strips in order to offer no lateral resistance. The concrete cylinder is actually cast-in-place against the pipe threads. Casting was carried out with the axis of the specimen placed vertically.

The radial confining pressure on the specimen is applied via a thin ring which surrounds the portion of pipe containing the concrete cylinder. A hydraulic jack with an adjustable relief valve closed the ring with a constant force during the test. In this way the longitudinal reaction and the radial confinement can be both controlled and measured independently of each other.

The concrete mix proportions were 1:3.02:1.35 for cement, sand, and 3/8-inch gravel, respectively. The water-cement ratio was 0.55. Three uniaxial compressive tests at 28 days on three 6-inch-tall, 3-inch-diameter cylinders yielded an average compressive strength of 4,220 psi. Three tensile splitting tests on the same specimen size yielded a tensile strength of 405 psi.

Bond Tests: Instrumentation and Procedure

On the loaded end of the bar, slip was measured using two LVDTs. They were diametrically opposed to compensate for any rotation. These LVDTs were clamped to the bar and measured the relative displacement of the outer concrete surface (i.e., the pipe). A third LVDT was located inside the pipe and measured the relative displacement (slip) between the pipe and the unloaded end of the bar. Finally, another LVDT measured the opening of the confining ring. This was later translated into a radial deformation. The apparatus was installed in a MTS testing machine. The MTS load cell provided pullout load measurements from which bond stresses were derived. A pressure gage was used to set the confining pressure.

Prior to each test, the concrete cylinder was precracked by setting a bar surface pressure of 500 psi and pulling on the bar until longitudinal splitting would occur. The specimen was then unloaded. After cracking, the confining pressure at the bar surface was set at either 500, 1,500, 2,500, 3,500, or 4,500 psi and kept constant during the remainder of the test. After cracking (and assuming that the cracks are open) all the pressure from the confining ring is

transferred to the bar. All tests were carried out in displacement control to obtain the unloading branches of the responses.

EXPERIMENTAL RESULTS

Tensile Test Results: Series 1

For each bar type, Table 2 shows the average properties obtained. The modulus of elasticity indicated is the secant modulus at a stress of 24 ksi. Stresses are obtained by dividing ultimate loads by the nominal cross section. Values in parenthesis are coefficients of variation. Figure 4 shows the stress-strain relationships for each bar.

It is observed that types A and C had similar moduli of elasticity and ultimate stresses. In addition, for these two types, results for all five bars were very consistent. Bar type D had a slightly lower modulus of elasticity but similar ultimate stress. Bar type B had very large scatter as indicated by the large coefficient of variation, with variations in modulus of elasticity and ultimate stress in excess of 50 percent (see Figure 4b). This was expected given the variation in cross-sectional area.

For each bar type, the following observations at failure are pertinent:

1. Type A - These bars have an additional layer consisting exclusively of matrix material around the fibers. This layer would tend to separate and initiate the bar failure, usually close to the grips. Subsequent to this separation, the bars could be reloaded to loads close to the ultimate. In all five tests, longitudinal splitting of the bar was observed which could be caused by a weak fiber-matrix interface (Ref 31).

2. Type B - The indentations produced sharp kinks in the longitudinal bar fibers. Bar failure was initiated by cracking at the kinks.

3. Type C - During the tests it was observed that the surface tow glued to the bar surface tended to get unbonded. In two cases, failure initiated at the grips. In all tests, longitudinal splitting of the bar was observed. Previous tests on these bars following ASTM D638-90 (Ref 24) yielded an average ultimate stress of 100 ksi and an elastic modulus of 6.1 Msi (Ref 17). Although this value for the modulus is similar to the present results, the ultimate stress is higher. This can be attributed to the difference in size between test specimens (in the ASTM D638-90 specimen only a 2.25-inch straight section was actually tested), and to the grip effects.

4. Type D - As in type B, bar failure usually initiated at the indentations. Previous tests on two 3/4-inch coupons following ASTM D638-90 were reported to yield ultimate stresses of 77.6 and 84.6 ksi, similar to the current average value (Ref 32).

Tensile Test Results: Series 2

Due to the grip effects encountered for Types A and C, three more tests were conducted for each one using specially designed grips. These grips had been initially designed for pulling the bars during the bond tests and are shown in Figure 3b. Results are shown in Table 3.

Although failure did still initiate at the grips in most cases, no early cracking or crushing sounds were perceived during the tests. Significantly higher ultimate stresses were measured for Type C (26 percent higher), which are now very close to the ones reported in Reference 17. For Type A, the increase was small, due again to the premature failure of the additional matrix layer.

Bond Test Results: Complete Bond Stress-Slip Curves

In the following, tests 1 through 5 for each bar type correspond to confining pressures at the bar surface of 500 through 4,500 psi (in 1,000-psi increments), as mentioned earlier. The slip mentioned in this section is the average measurement of the two LVDTs located on the loaded end of the bar. This measurement was corrected for the unbonded length of rebar and the gage offset.

Figure 5 shows the complete bond stress versus loaded-end slip response. Figure 6 shows the variation in bond strength (i.e., peak bond stress) versus radial confining pressure. Both values are normalized by the tensile strength (405 psi). Figure 7 shows the same data together with previous data for steel bars (Refs 25 through 27) (in this figure the points are only markers, not data points). Figure 8 shows some tests repeated for evaluation of indentation depth effects. The following was observed for each bar type:

1. Type A - In test 5 of type A (missing from Figure 5a), the concrete cylinder appeared weaker and those results were discarded. Although the concrete specimen was subjected to a confining pressure of 4,500 psi at the bar surface in excess of the uniaxial compressive strength, in most cases this did not result in crushing (due to the multiaxial confinement).

It was apparent that the response was qualitatively similar to that of steel (Refs 25 through 27). The bond strength increased significantly with confinement. At a slip approximately equal to the clear deformation spacing, the bond stress remained fairly constant.

2. Type B - Although the bond strength also increased with confining pressure, a large scatter was present. For test 5, the bar had much greater indentations, yielding an unexpectedly high bond strength. Also, the peaks occurred at a variety of different slip magnitudes.

3. Type C - In these tests the concrete cylinder never split, so most of the confining pressure was carried by the concrete cylinder as hoop stress. Consequently, the response was almost not affected by confinement. The response exhibited a high initial adhesion followed by a constant bond stress for all five tests.

It was observed that the deformations initially glued to the bar debonded during the test. Consequently, the bond stress was dependent on the friction between the bar and the concrete (i.e., on the roughness of the sand coating). This would explain why Reference 16 reports: (1) a high increase in pullout load when the sand coating is present, and (2) no significant increase when the deformations pitch is reduced. However, in Reference 16, the deformations may not have debonded since the shape of the reported pullout load-slip curve indicates deformation locking, and the bond stresses reported are higher. In any case, the bond response is dependent on the adhesion between the deformations and the bar, and the capacity of this adhesion is not easily determined.

4. Type D - The bond strength increase with confinement was smooth. A sudden drop in bond stress was observed at about 3/4 inch.

5. Confinement Effects on Bond Strength - Figure 6 shows that for types A, B, and D the bond strength can be significantly affected by the bar confinement. For type D, the bond strength increased fourfold when the radial pressure on the bar was increased from 500 to 4,500 psi. For types A and B, the increase was closer to threefold.

Figure 7 compares these results with previous data obtained for steel rebars (Refs 25 through 27). It is seen that the maximum normalized bond strengths obtained were similar in magnitude (between 4 and 5) although they were obtained at higher confinement values. For a given confinement, the bond strength developed by a steel bar was between 1.2 and 1.5 times higher than that of the equivalent FRP bar.

6. Effect of Indentation Depth - Two additional tests for types B and D were run as a means of evaluating the effects of indentation depth on the results.

For type B, a bar was chosen among the ones with shallowest indentations. For this bar, the indentation depth was only 0.022 inch. This test (test 3a) was carried out at a confinement of 2,500 psi to compare with test 3 where the bar had an average indentation depth of 0.057 inch (test 5 indentation depth was 0.088 inch). Figure 8a shows that the decrease in indentation depth is accompanied by a bond strength decrease of 18.4 percent.

Similarly for type D, a second test (test 2a) was carried out at a confinement of 1,500 psi. The bar in test 2a had an indentation depth of 0.051 inch versus 0.071 inch for test 2. Figure 8b shows a corresponding decrease in bond strength of 16.2 percent.

Bond Test Results: Initial Bond Stress-Slip Curves

Upon starting the loading, the two LVDTs on the loaded end of the rebar started measuring displacement, however, the internal LVDT on the unloaded end did not record any movement for some time. During this initial phase, the slip was nonuniform within the five-lug test section of the rebar. This was in contrast with the end of the test where all three LVDTs recorded almost equal slips. References 29 and 30 show the evolution of the slip distribution along the test length. For the beginning of the loading it indicates that the average slip within the test length is approximately equal to:

$$\text{Average initial slip} = (2s_2 + s_1)/3$$

where s_1 = average slip from two loaded end LVDTs
s_2 = slip from unloaded end (internal) LVDT

Figure 9 shows the initial bond stress-slip curves using the average initial slip defined. The following observations are pertinent:

- All curves show some adhesion between 100 and 300 psi (i.e., a bond stress at zero slip).

- Beyond this adhesion, the slope of the curve appears to increase with higher confinement.

Bond Test Results: Bond Stress-Radial Displacement Curves

Upon first loading, the rebar deformations exert radial pressures against the surrounding concrete until the latter splits longitudinally. If external confinement is provided (as in the present case), the rebars tend to slowly open the concrete cracks until enough space is created for the lugs to advance, via a combination of sliding and concrete crushing. Eventually, after enough crushing has taken place, a radial contraction may occur (Refs 25 through 27). To capture this dilation, the ring opening was measured, which was converted to a radial displacement at the outer surface of the concrete cylinder specimen. The bond stress versus radial displacement curves obtained are shown in Figure 10.

For each rebar type the following was observed:

1. Type A - A standard response, similar to that of steel (Ref 25), was obtained, where radial dilation took place, mainly past the peak stress, then a fairly constant maximum opening was reached, and was usually followed by a contraction. The contraction was most visible in test 1, whereas the constant maximum opening was more obvious in tests 2 and 3. In test 4, the external pressure was high enough to prevent any dilation and allow only for some contraction at the end of the test. The maximum dilation reached decreased rapidly with increasing confining pressure.

2. Type B - A similar response was obtained. Larger dilation was obtained due to the presence of large indentation depths.

3. Type C - No dilation was apparent, consistent with the fact that the concrete cylinders never split.

4. Type D - No contraction was apparent at the end of the tests probably due to the fact that the final slip was much smaller than the indentation spacing for this bar type. Some scatter was present as shown by the fact that test 3 had a greater maximum dilation that test 2. No dilation was present for the higher confining pressures.

Bond Test Results: Interface Examination

In all specimens (except type C), three or more evenly spaced longitudinal cracks would form during the first loading cycle. At low confining pressures, there were usually three cracks, and large crack openings would be present at the end of the test (Figure 11a). At high confining pressures, four to six longitudinal cracks would form, with smaller openings. The specimens were consequently opened to observe the interface condition. The first observation was the absence of radial cracks which are significant in the case of steel bars (Refs 25 through 27). For each bar type, the following was also noted:

1. Type A - Figure 11b shows that the concrete at the indentations was crushed and the resin cover between indentations suffered significant damage. The underlying fibers appeared to have been protected.

2. Type B - Figure 11c shows similar results although fibers between indentations were sheared off.

3. Type C - For this rebar type, the specimens did not crack longitudinally during the tests, but they were cracked into two pieces a posteriori to observe the interface.

In Figure 11d it can be seen that the deformations fractured near the loaded end. The longitudinal distance between both sides of the fracture is equal to the final slip. Both the deformations and the sand coating within the concrete cylinder remained perfectly bonded to the concrete and separated from the longitudinal fibers. The other side of the fractured deformation moved out with the bar. At the unloaded end of the specimen, all the deformations which should have advanced collapsed together. This failure mechanism took place in all specimens of this type.

4. Type D - Figure 11e shows that the protective veil was separated from the rest of the bar. This was apparent in two specimens.

ANALYTICAL MONOTONIC ENVELOPE

An analytical expression for the monotonic bond stress-slip curve would be useful to extend the present results to situations with generic confinement and different concrete strength. This expression is derived in a two-step procedure. First, the peak on the bond stress-slip curve is defined as a function of confinement as follows:

$$\tau_m/f_t = A + B\,(1 - e^{-C\sigma/f_t})$$

$$\delta_m = D + E\,\sigma$$

where τ_m = bond strength (peak bond stress)

σ = confining axisymmetric radial pressure

f_t = tensile strength

δ_m = slip at peak bond stress

A,B,C,D,E = empirical constants for each bar type

Second, the complete normalized bond stress-slip curve can be expressed as $\tau = \tau(\delta,\sigma)$:

$$\tau = \tau_m \frac{F\,(\frac{\delta}{\delta_m}) + (G - 1)\,(\frac{\delta}{\delta_m})^2}{1 + (F - 2)\,(\frac{\delta}{\delta_m}) + G\,(\frac{\delta}{\delta_m})^2}$$

where F,G = empirical constants for each bar type

The constants were evaluated for bar types A and D, as well as for the two types of steel bars from Referencse 25 through 27 (with lugs inclined at 68 and 90 degrees, respectively, with the longitudinal axis). The results are as follows:

Bar Type	A	B	C	D	E	F	G
Type A	1.00	9.04	0.05	0.0202	5.87E-6	11.0	1.2
Type D	0.266	5.63	0.15	0.0475	5.23E-5	13.0	0.5
Steel 68° lugs	0.9	3.5	0.35	0.0209	5.32E-6	9.0	0.65
Steel 90° lugs	0.9	4.4	0.35	0.0053	8.50E-6	5.5	1.1

These analytical fits are compared to the actual data for type A in Figure 12a. Figure 12b compares the fits of type A and of the 68-degree lug steel bar for a fictitious concrete with tensile stre. ... f_t = 500 psi and three values of the confining pressure σ: 1,500, 2,500, and 3,500 psi. In the fits, the bond stress is assumed to remain constant after the slip has reached the clear deformation spacing or the indentation spacing.

CONCLUSIONS

Four different fiber-reinforced glass rebar types with different deformations were analyzed to derive their bond characteristics. Local bond stress-slip and bond stress-radial displacement curves were obtained for various levels of axisymmetric radial confining pressure. It was found that:

1. Small surface deformations, about 5.4 percent of the nominal rebar diameter (i.e., similar to that of steel), are sufficient to yield bond stresses up to five times the concrete tensile strength, similar to that obtained with steel rebars. Either surface deformations or indentations obtained by stressing an external helicoidal strand are acceptable for bond purposes. Deformations just glued to the surface are not recommended since they may become unbonded and thereafter fail to provide any bond per se.

2. For the same amount of confinement, the bond strength in a steel bar is, on the average, 1.2 to 1.5 times greater than the bond strength on a FRP rebar (for the cases studied).

3. Large variations in the indentation depths result in large variations in bond strength.

4. Bond strength can usually be increased threefold by increasing confining pressure.

REFERENCES

1. B.S. Hamad, J.O. Jirsa, and N. D'Abreu de Palo. "Anchorage strength of epoxy-coated hooked bars," ACI Structural Journal, vol 20, no. 2, Mar-Apr 1993, pp 210-217.

2. D.P. Gustafson. "Epoxy update," Civil Engineering, ASCE, vol 58, no. 10, Oct 1988, pp 38-41.

3. D. Darwin, S.L. McCabe, H. Hadje-Ghaffari, and O.C. Choi. "Bond strength of epoxy-coated reinforcement to concrete - An update," Serviceability and Durability in Construction Materials, in Proceedings of the First Materials Engineering Congress, Denver, CO, Aug 1990, pp 115-124.

4. University of Kansas Center for Research. SM Report No. 28: Effects of epoxy-coating on the bond of reinforcing steel to concrete, by H. Hadje-Ghaffari, D. Darwin, and S. McCabe. Lawrence, KS, Jul 1991.

5. C.A. Ballinger. "Development of composites for civil engineering," in Proceedings of the Conference on Advanced Composite Materials in Civil Engineering Structures, ASCE, Las Vegas, NV, 1991, pp 288-301.

6. H. Saadatmanesh and M.R. Ehsani. "Application of fiber-composites in civil engineering," Structural Materials, in Proceedings of the Structures Congress 1989, ASCE, San Francisco, CA (J.F. Orofino, ed.), May 1989, pp 526-535.

7. R. Sen, S. Iyer, M. Issa, and M. Shahawy. "Fiberglass pretensioned piles for marine environment," in Proceedings of the Conference on Advanced Composite Materials in Civil Engineering Structures, ASCE, Las Vegas, NV, 1991, pp 348-359.

8. R. Wolff and H.J. Miesseler. "New materials for prestressing and monitoring heavy structures," Concrete International, vol 11, no. 9, Sep 1989, pp 86-89.

9. C.W. Dolan. "Developments in non-metallic prestressing tendons," PCI Journal, Sep-Oct 1990, pp 80-88.

10. H.J. Miesseler and R. Wolff. "Experience with fiber composite materials and monitoring with optical fiber sensors," in Proceedings of the Conference on Advanced Composite Materials in Civil Engineering Structures, ASCE, Las Vegas, NV, 1991, pp 167-181.

11. C.H. Goodspeed, G. Aleva, and E. Shmeckpeper. "Bridge deck test facility for FRP reinforced bridge deck panels," Use of Composite Materials in Transportation Systems, AMD-vol 129, Winter Annual Meeting, ASME, pp 73-76.

12. J. Larralde and R. Siva. "Bond stress-slip relationships of FRP rebars in concrete," Serviceability and Durability in Construction Materials, in Proceedings of the First Materials Engineering Congress, Denver, CO, Aug 1990, pp 1134-1141.

13. S. Iyer and M. Anigol. "Testing and evaluating fiberglass, graphite, and steel prestressing cables for pretensioned beams," in Proceedings of the Conference on Advanced Composite Materials in Civil Engineering Structures, ASCE, Las Vegas, NV, 1991, pp 44-56.

14. L.G. Pleimann. "Strength, modulus of elasticity, and bond of deformed FRP rods," in Proceedings of the Conference on Advanced Composite Materials in Civil Engineering Structures, ASCE, Las Vegas, NV, 1991, pp 99-110.

15. S. Tao, M.R. Ehsani, and H. Saadatmanesh. "Bond strength of straight GFRP rebars," Materials Performance and Prevention of Deficiencies and Failures, in Proceedings of the Materials Engineering Congress, ASCE, Atlanta, GA, 1992, pp 598-605.

16. O. Challal and B. Benmokrane. "Pullout and bond of glass-fibre rods embedded in concrete and cement grout," Materials and Structures, vol 26, Apr 1993, pp 167-175.

17. O. Challal and B. Benmokrane. "Glass-fiber reinforcing rod: Characterization and application to concrete structures and grouted anchors," Materials Performance and Prevention of Deficiencies and Failures, in Proceedings of the Materials Engineering Congress, ASCE, Atlanta, GA, 1992, pp 606-617.

18. O. Challal, B. Benmokrane, and R. Masmoudi. "An innovative glass-fire composite rebar for concrete structures," Advanced Composite Materials in Bridges and Structures, First International Conference, Sherbrooke, Quebec, Canada, 1992, pp 169-177.

19. S. Daniali. "Development length for fibre-reinforced plastic bars," Advanced Composite Materials in Bridges and Structures, First International Conference, Sherbrooke, Quebec, Canada, 1992, pp 179-188.

20. C. Ballinger. "Structural FRP composites," Civil Engineering, ASCE, vol 60, no. 7, Jul 1990, pp 63-65.

21. P. Tarricone. "Plastic potential," Civil Engineering, vol 63, no. 8, Aug 1993, pp 62-63.

22. American Society for Testing and Materials. ASTM A615-89: Standard specification for deformed and plain billet-steel bars for concrete reinforcement, Annual Book of ASTM Standards, vol 01.04, 1990.

23. _____. ASTM D3916-84: Test method for tensile properties of pultruded glass-fiber-reinforced plastic rod, Annual Book of ASTM Standards, vol 08.03, 1991.

24. _____. ASTM D638-90: Test method for tensile properties of plastics, Annual Book of ASTM Standards, vol 08.01, 1991.

25. L.J. Malvar. "Confinement stress dependent bond behavior, Part I: Experimental investigation," Bond in Concrete, in Proceedings of the International Conference, Riga, Latvia, Oct 1992, pp 1/79-1/88.

26. L.J. Malvar. "Bond of reinforcement under controlled confinement," ACI Materials Journal, vol 89, no.6, Nov-Dec 1992, pp 593-601.

27. L.J. Malvar. "Bond of reinforcement under controlled radial pressure," Studi e Ricerche, vol 13-1992, Structural Engineering Department, Polytechnic University of Milan, Milan, Italy, 1992, pp 83-118.

28. J.V. Cox and L.R. Herrmann. "A plasticity model for the bond between matrix and reinforcement," in Proceedings of the 6th U.S.-Japan Conference on Composite Materials, Orlando, FL, Jun 1992.

29. J.V. Cox and L.R. Herrmann. "Confinement stress dependent bond behavior, Part II: A two degree of freedom plasticity model," Bond in Concrete, in Proceedings of the International Conference, Riga, Latvia, Oct 1992, pp 11/11-11/20.

30. J.V. Cox. Development of a plasticity bond model for reinforced concrete - theory and validation for monitonic applications, Ph.D. thesis, University of California, Davis, CA, 1994 (in preparation).

31. S.H. Saidpour. The effect of fibre/matrix interfacial interactions on the mechanical properties of unidirectional E-glass reinforced vinyl ester composites, Ph.D. thesis, Loughborough University of Technology, U.K., 1991.

32. DNV Industrial Services. Tensile test results on nominal 3/4-inch FRP rebar. Houston, TX, 1988.

Table 1
Geometrical Properties

Bar Type (3/4-inch diameter)	Deformation or Indentation Spacing (in.)	Deformation Height or Indentation Depth (in.)
A	0.72 (0.96 ⌀) ± 13.8%	0.041 (0.054 ⌀) ± 7.5%
B	0.94 (1.25 ⌀) ± 1.9%	0.063 (0.084 ⌀) ± 51.8%
C	0.78 (1.03 ⌀) ± 2.3%	0.047 (0.067 ⌀) ± 2.8%
D	1.35 (1.80 ⌀) ± 7.6%	0.069 (0.092 ⌀) ± 13.7%
Steel	<0.525 (0.70 ⌀)	>0.038 (0.0507 ⌀)

Table 2
Mechanical Properties, Series 1

Bar Type	Modulus of Elasticity (Msi)	Ulitmate Stress (ksi)	Ultimate Strain (%)
A	6.74 (± 1.3%)	86.7 (± 2.2%)	1.41 (± 3.4%)
B	4.10 (± 22.6%)	65.1 (± 20.7%)	1.73 (± 11.2%)
C	6.88 (± 2.4%)	81.4 (± 5.1%)	1.23 (± 6.5%)
D	5.77 (± 2.2%)	81.3(± 2.2%)	1.79(± 3.8%)

Table 3
Mechanical Properties, Series 2

Bar Type	Ultimate Stress (ksi)
A	89.5 (± 2.7%)
C	103.0 (± 5.1%)

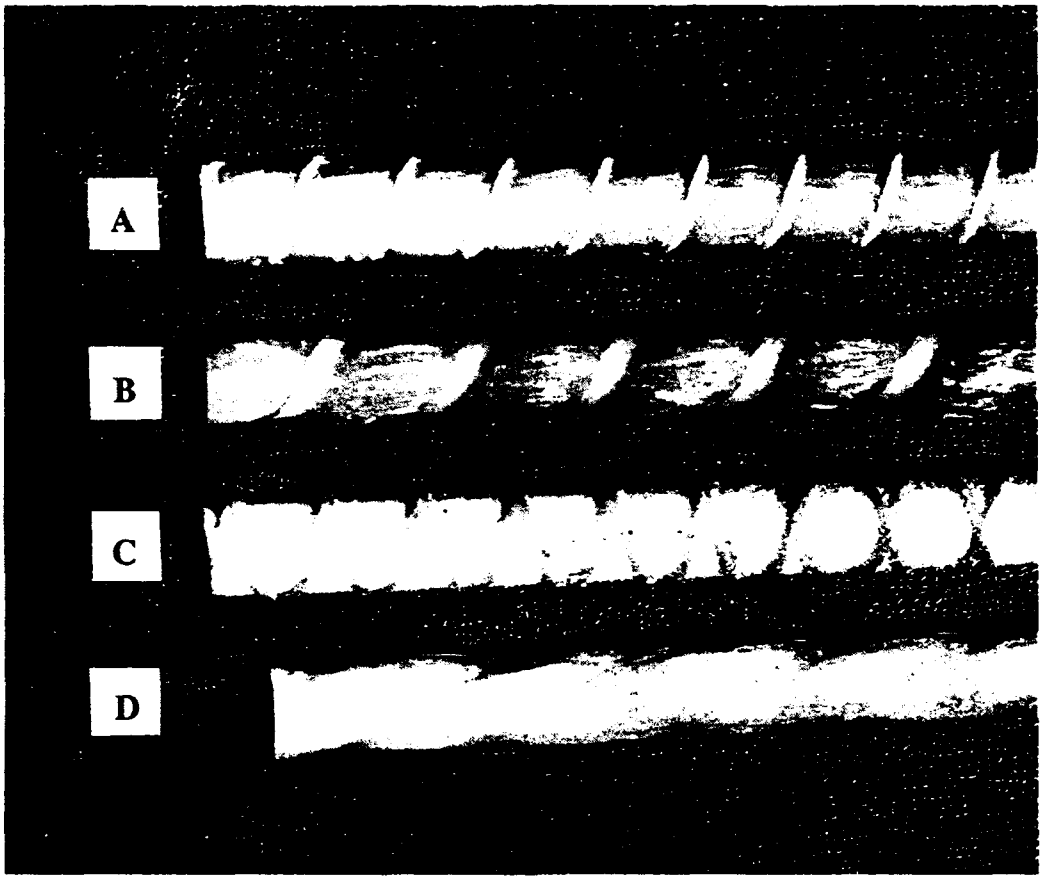

Figure 1
Bar types.

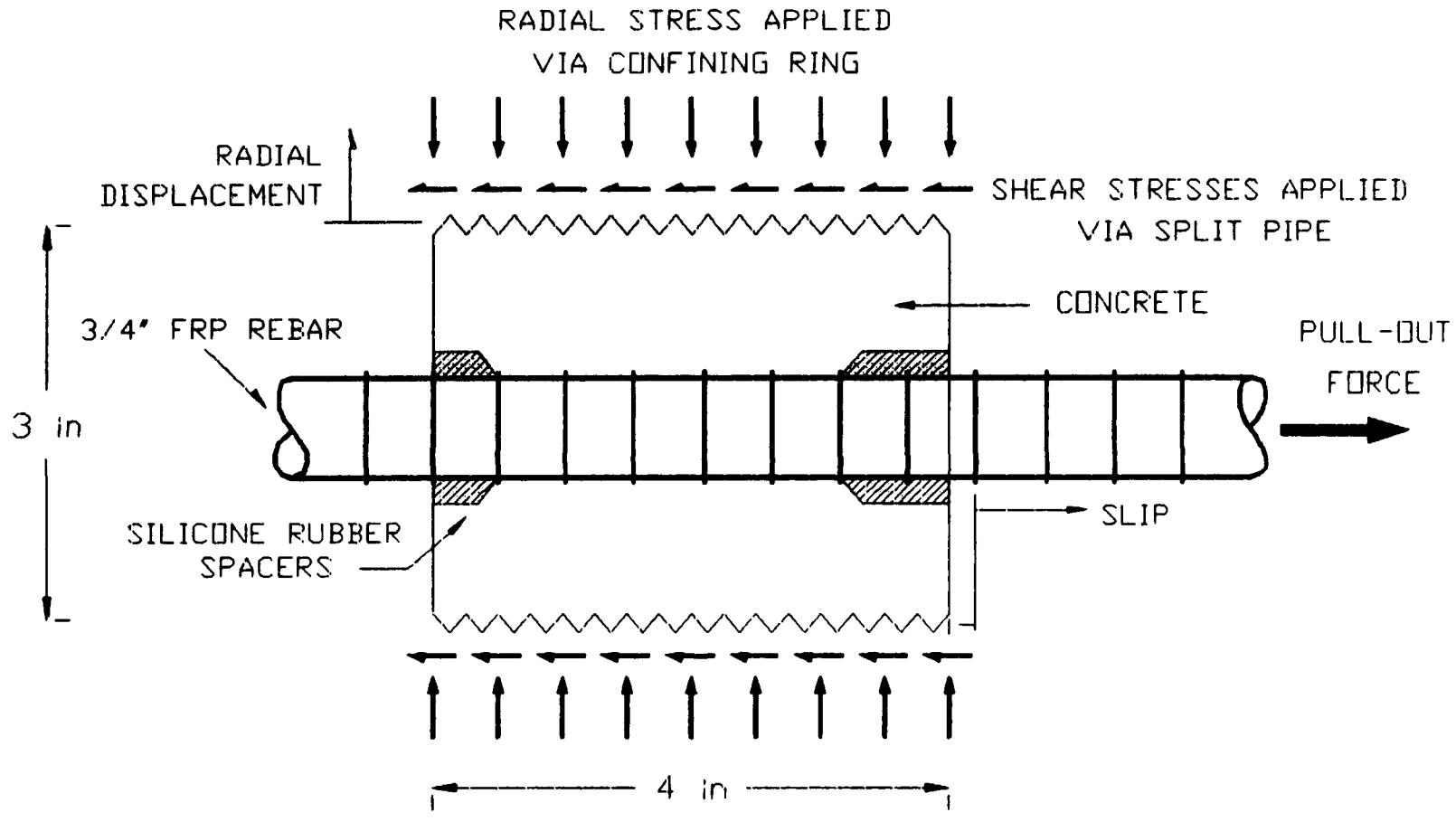

Figure 2
Test specimen.

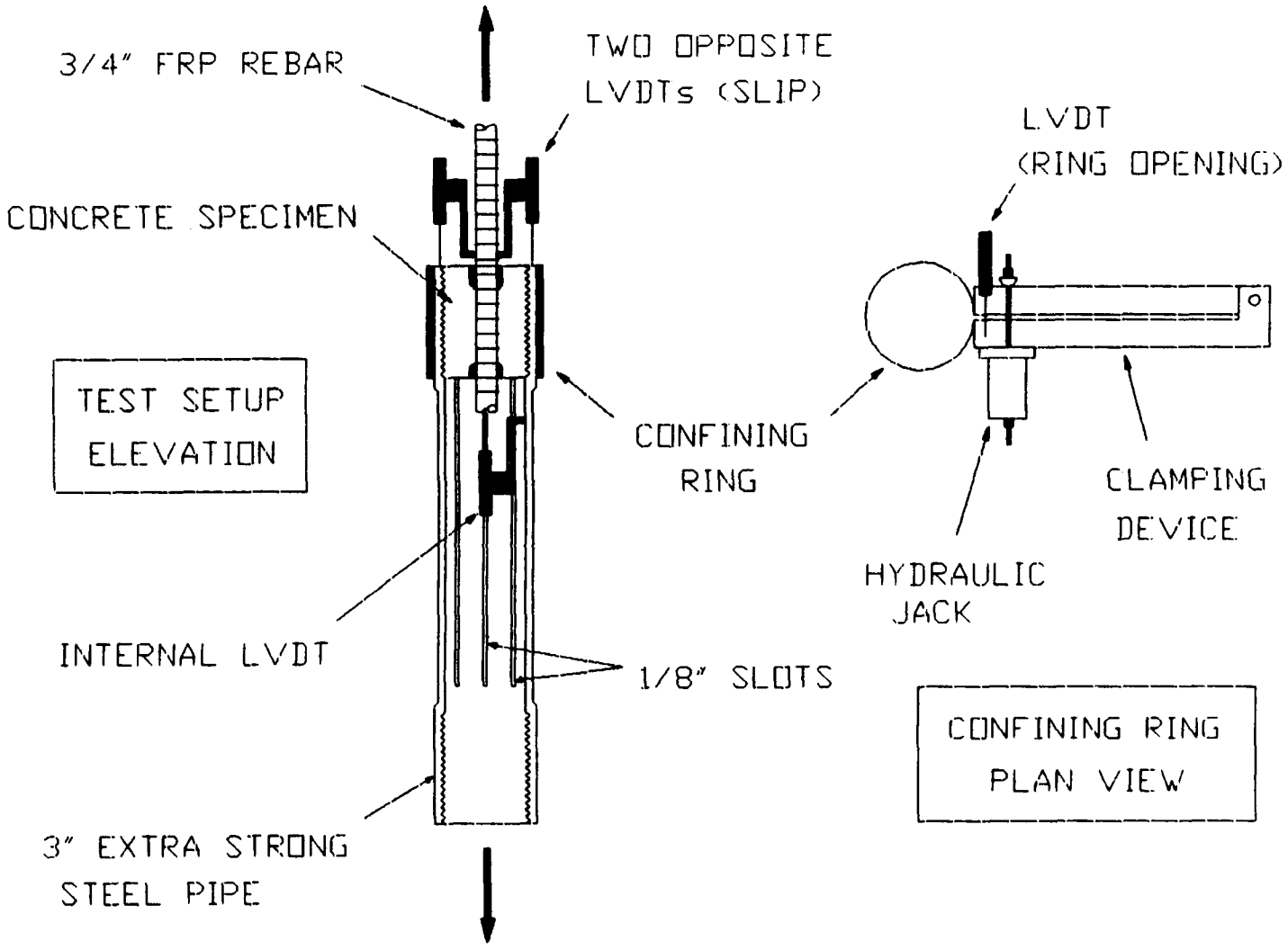

Figure 3a
Test setup and confining ring.

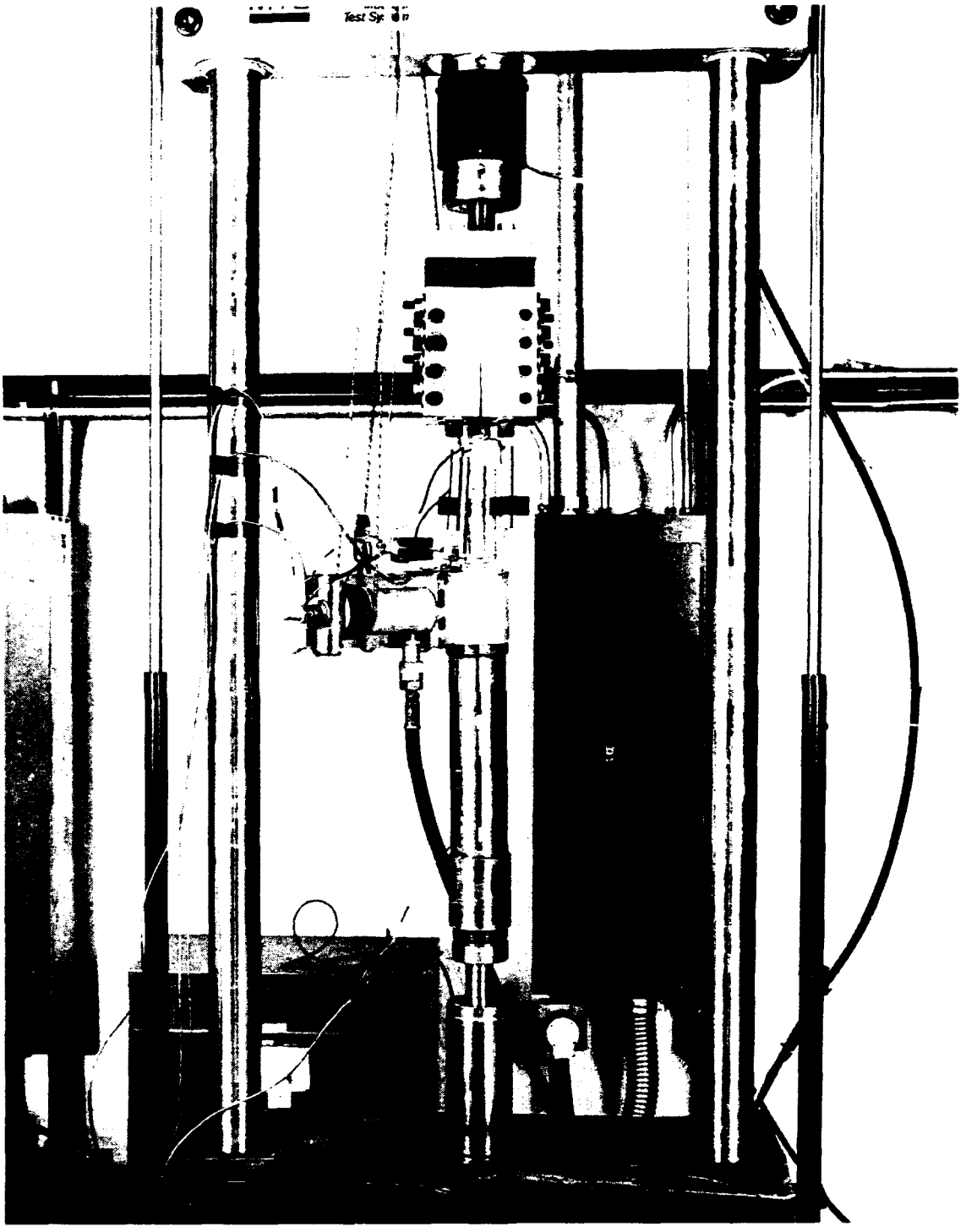

Figure 3b
Photograph of setup.

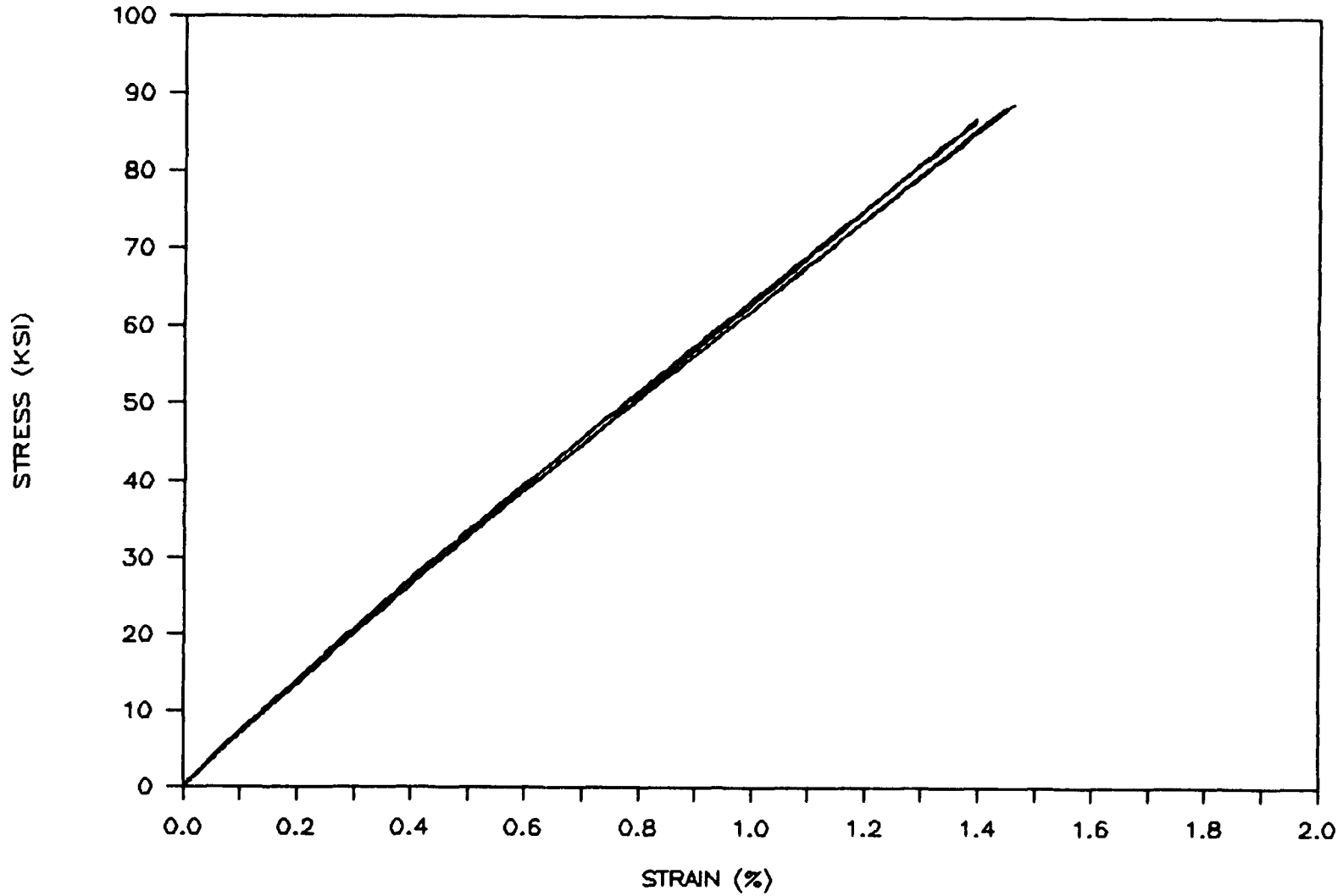

Figure 4a
Tensile tests results: type A.

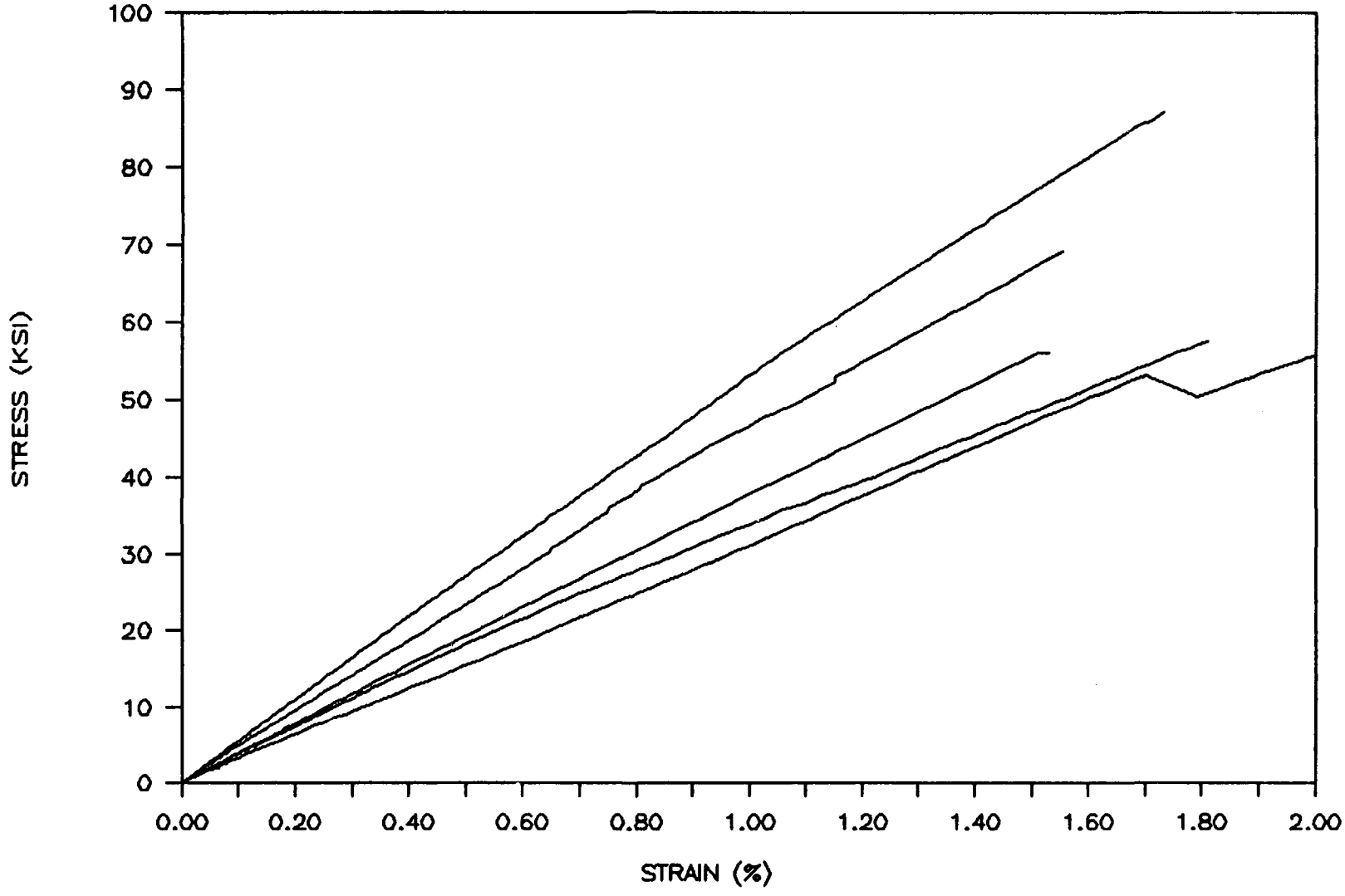

Figure 4b
Tensile tests results: type B.

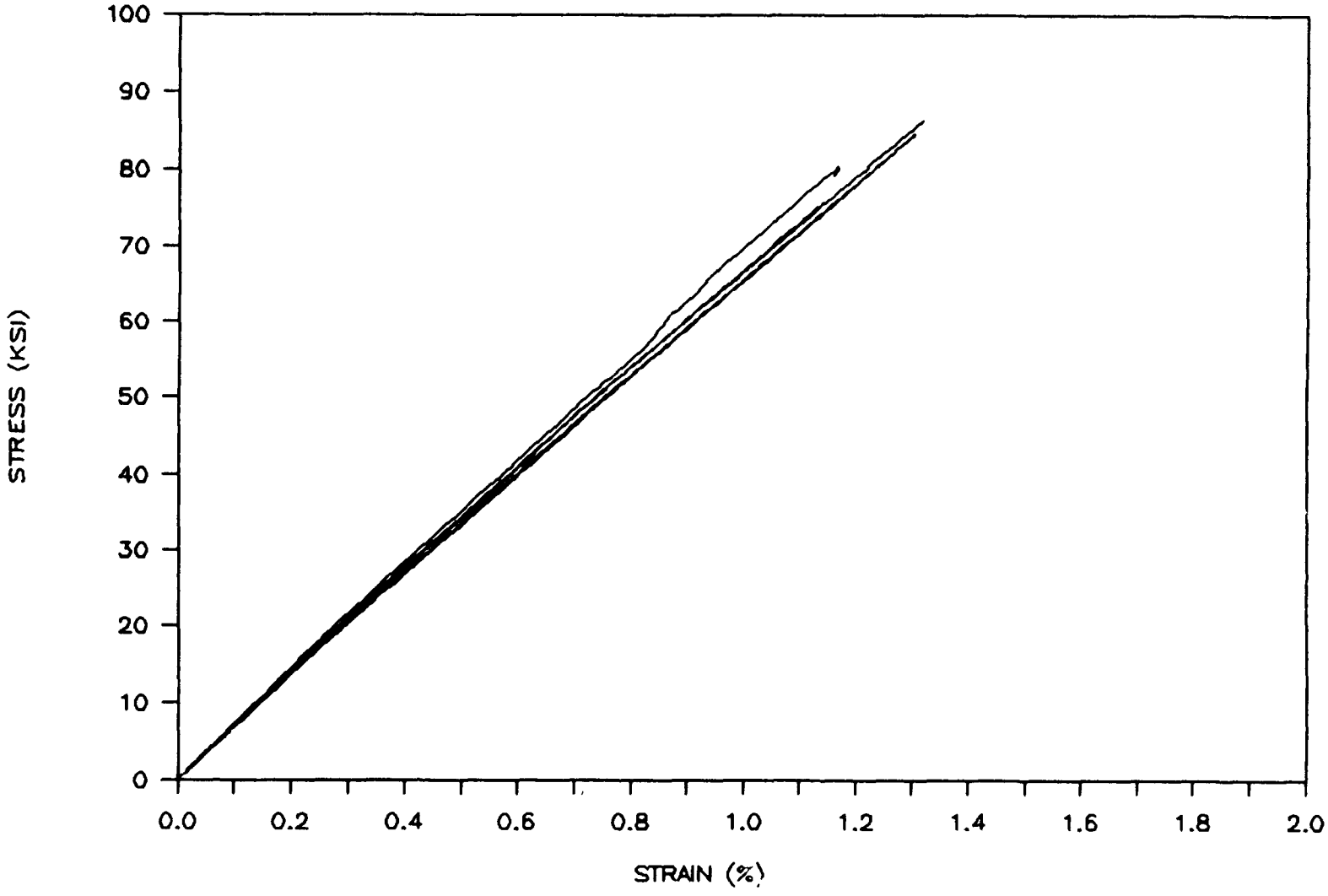

Figure 4c
Tensile tests results: type C.

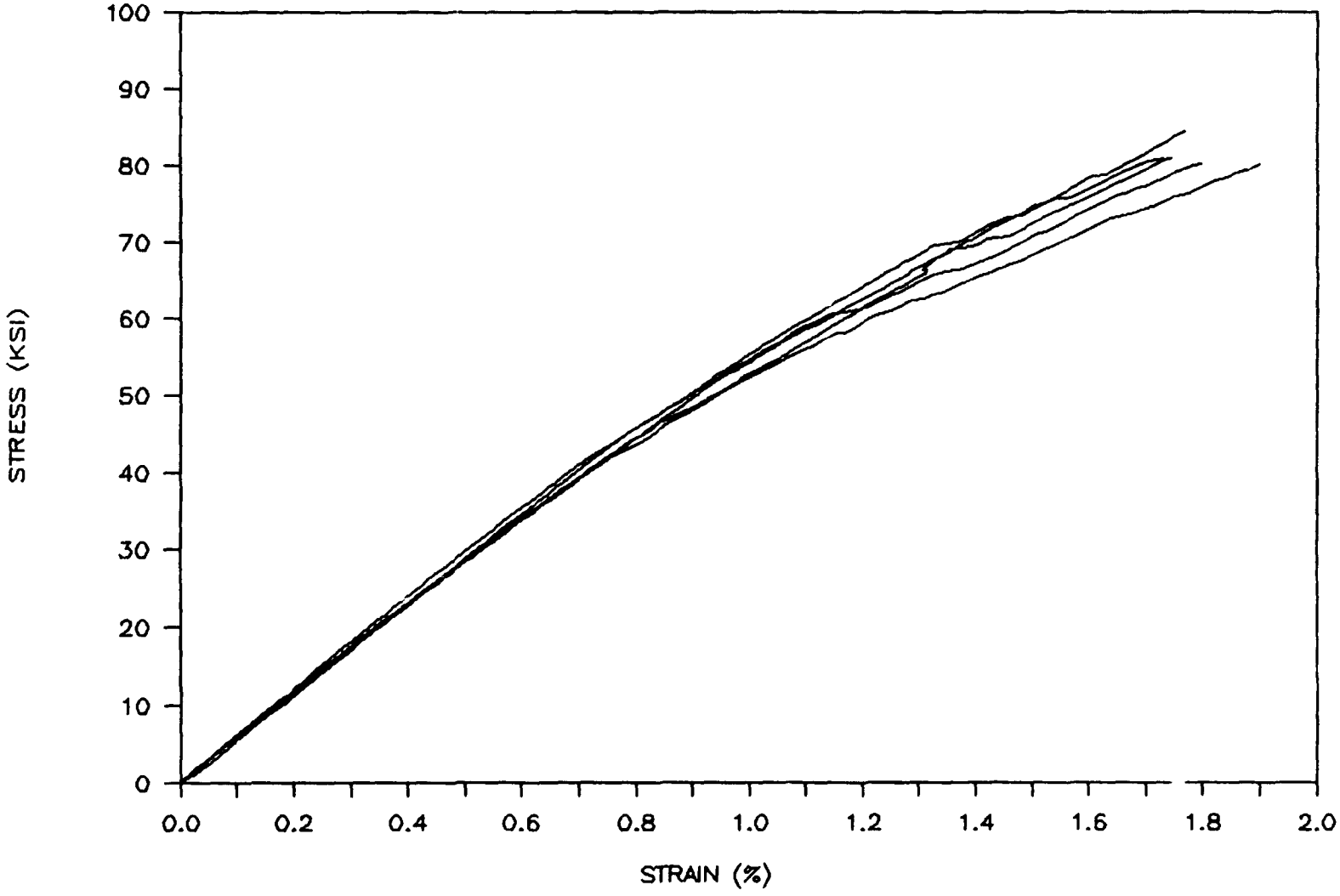

Figure 4d
Tensile tests results: type D.

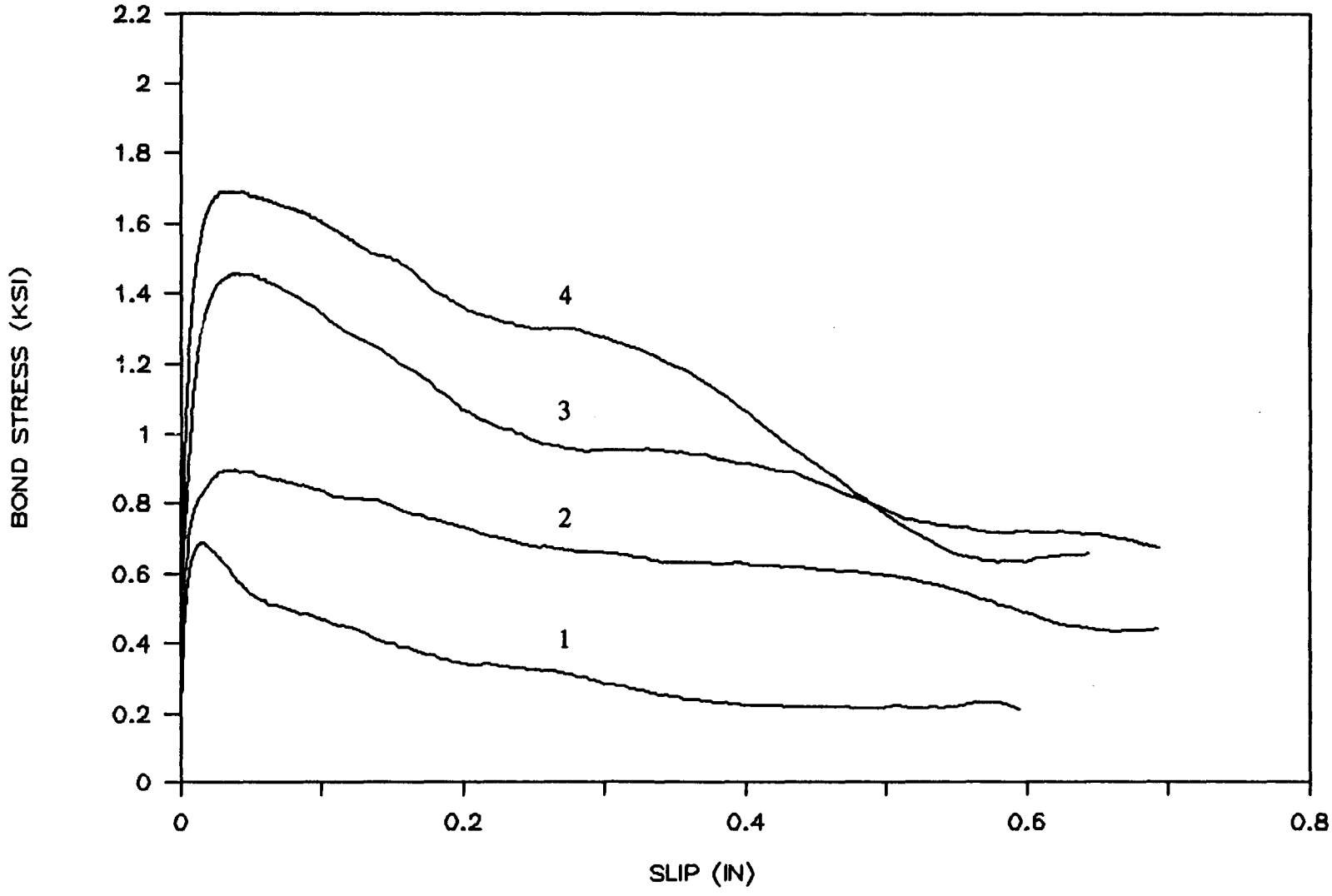

Figure 5a
Complete bond stress-slip curves: type A.

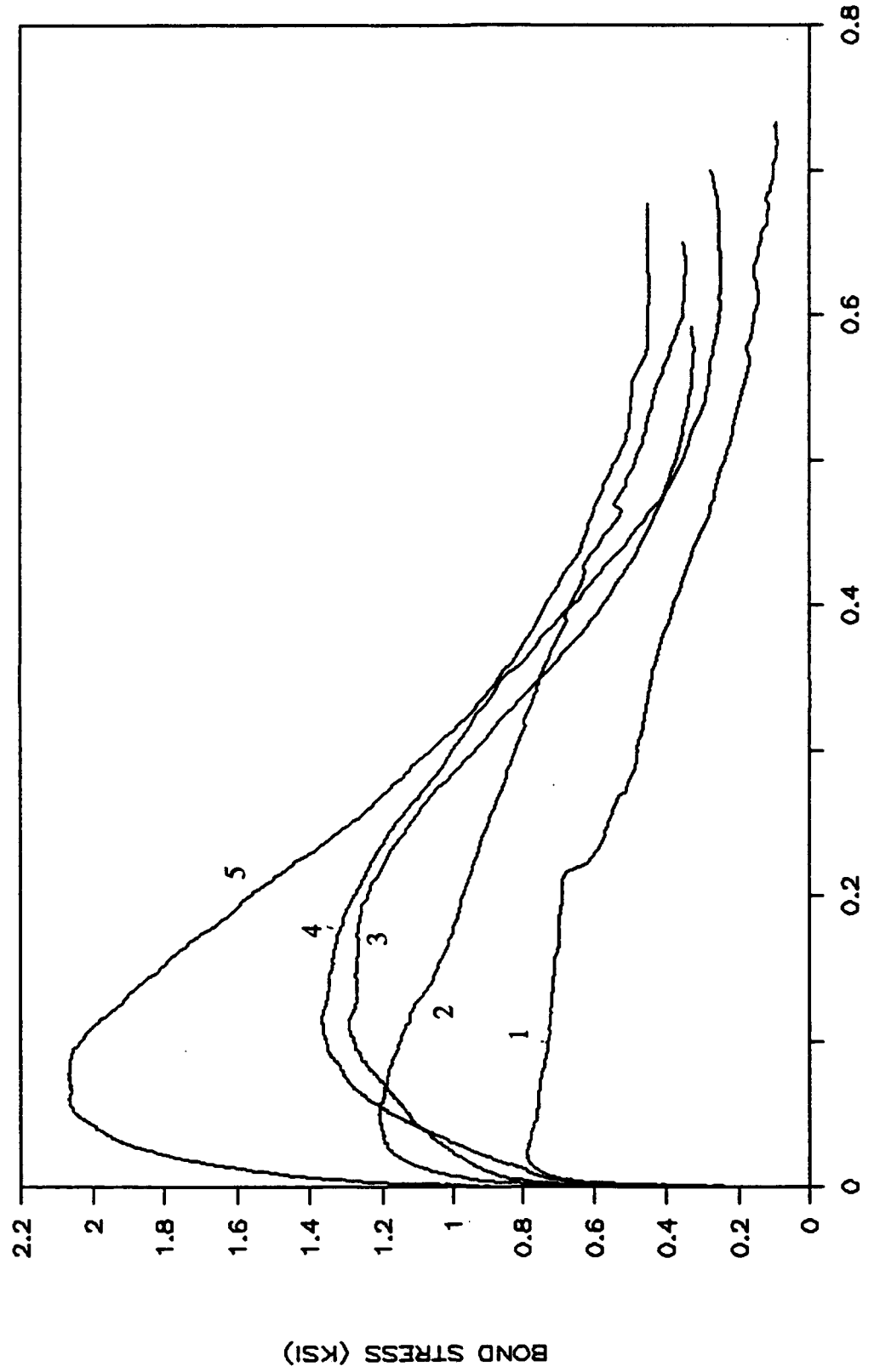

Figure 5b
Complete bond stress-slip curves: type B.

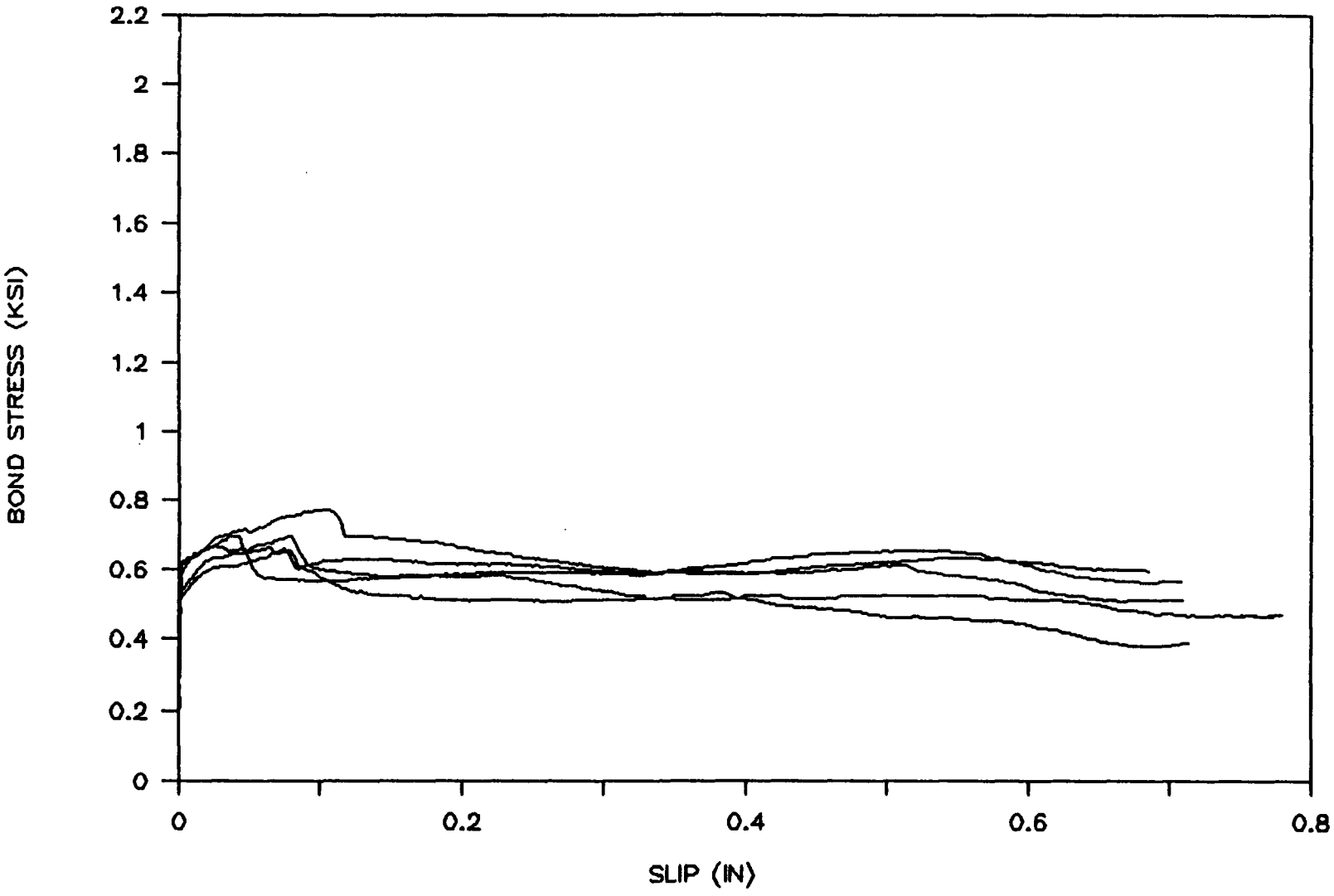

Figure 5c
Complete bond stress-slip curves: type C.

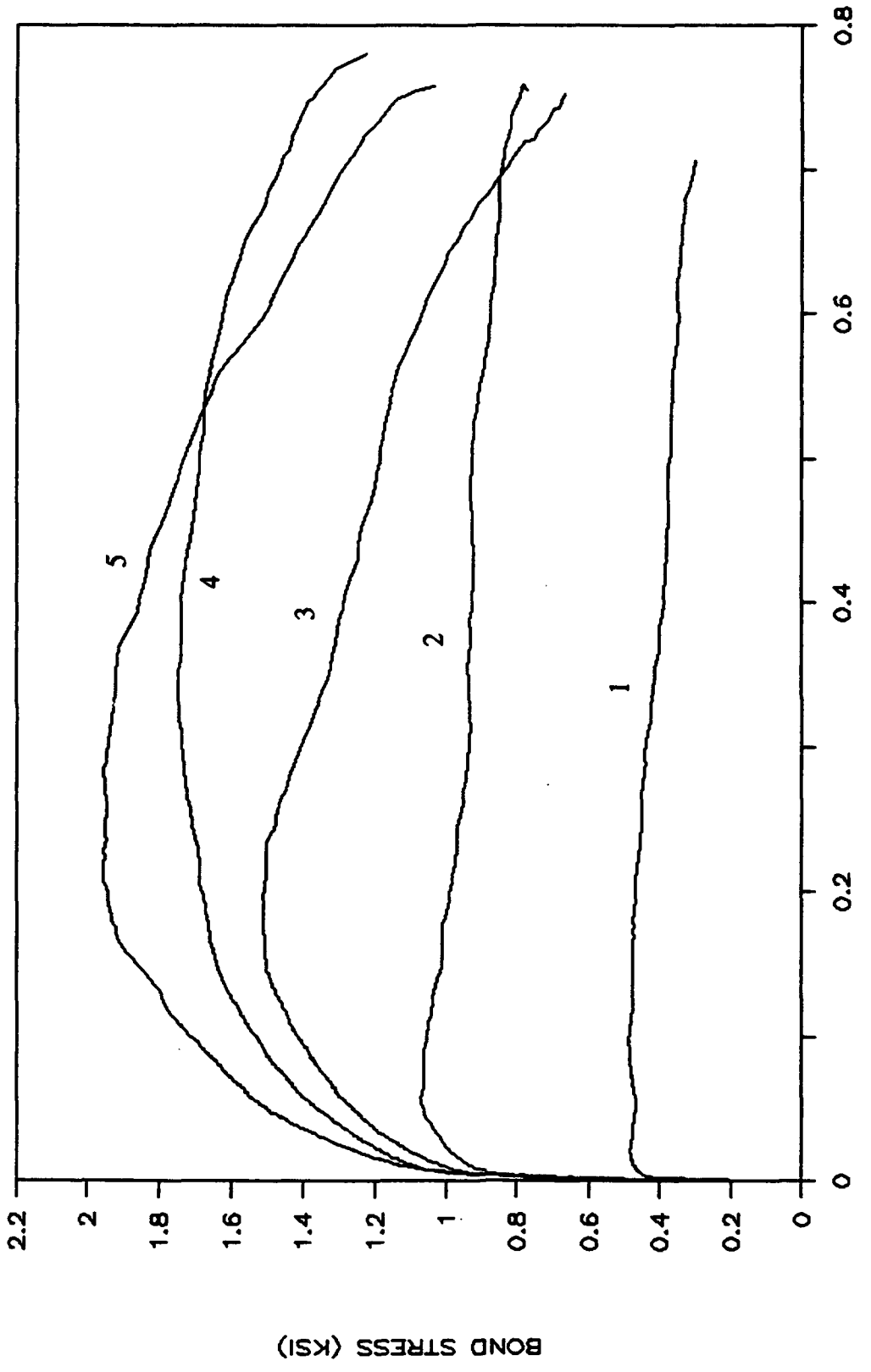

Figure 5d
Complete bond stress-slip curves: type D.

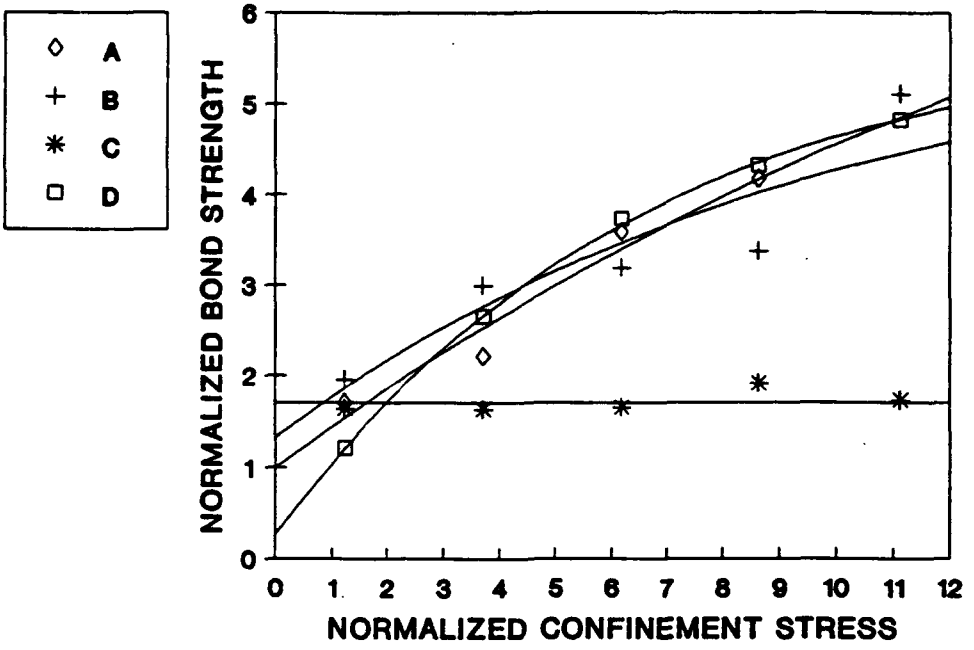

Figure 6
Effect of confinement on bond strength.

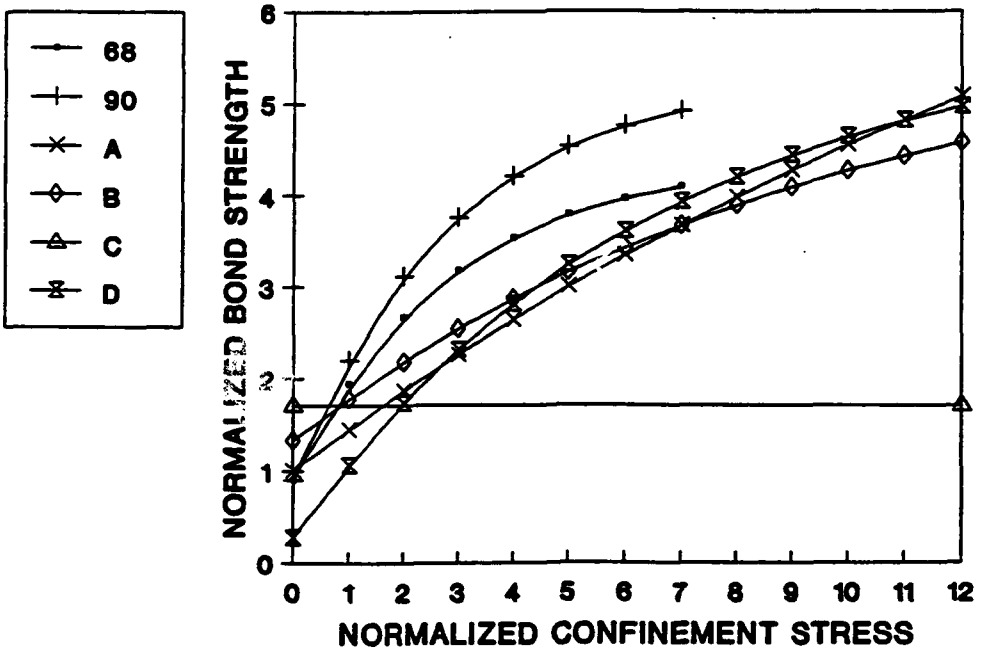

Figure 7
Bond strength: comparison to previous steel results.

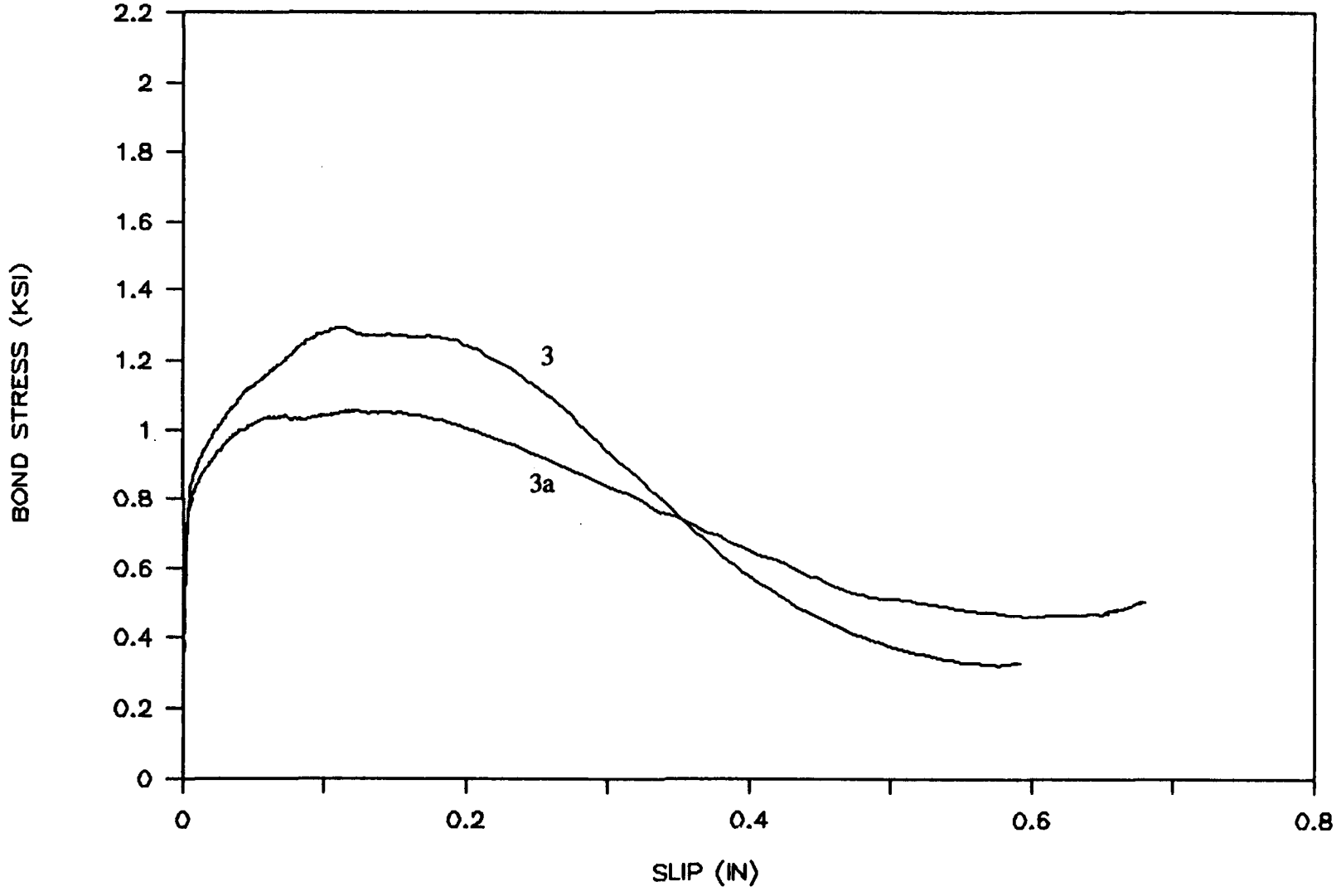

Figure 8a
Scatter in bond tests: type B.

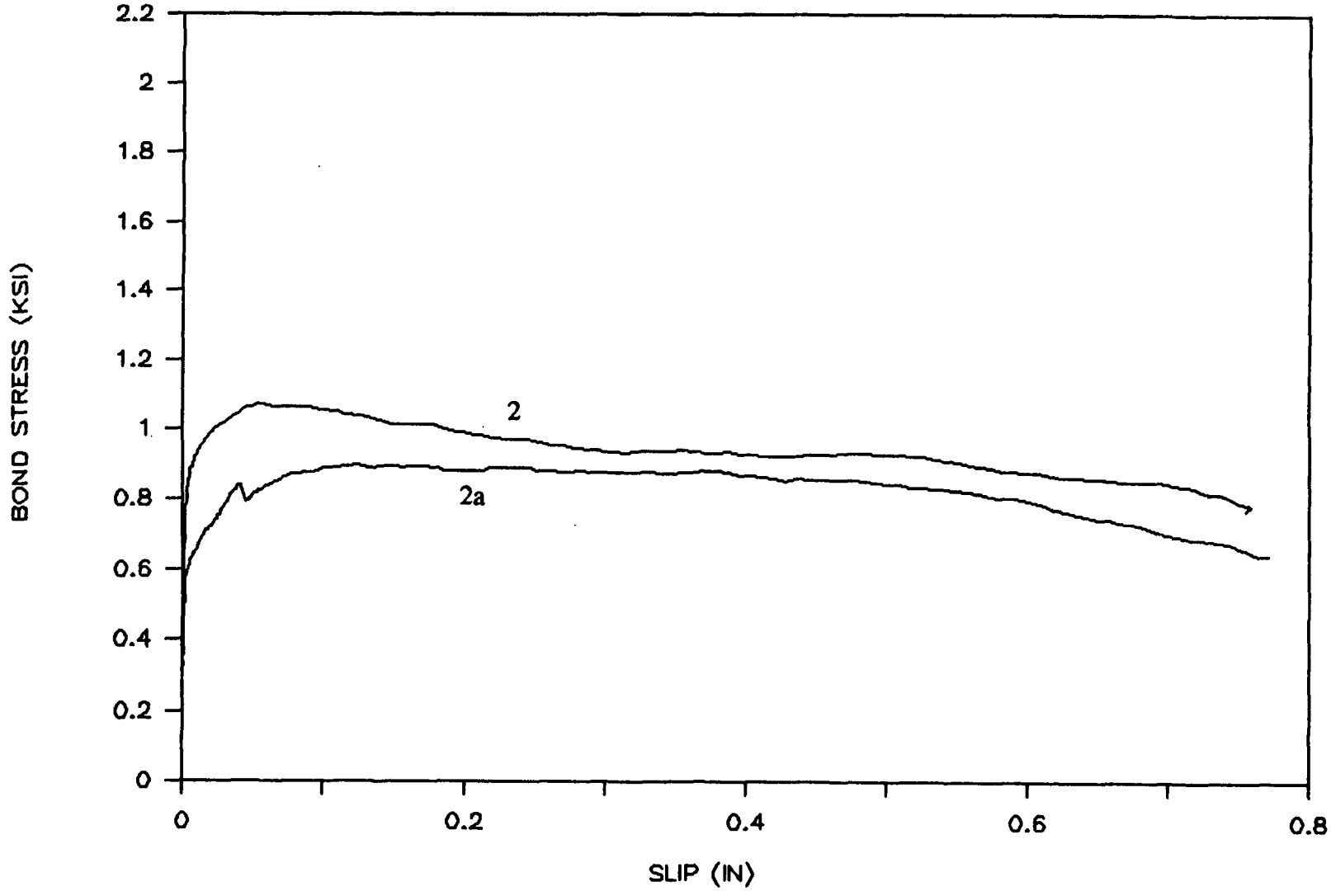

Figure 8b
Scatter in bond tests: type D.

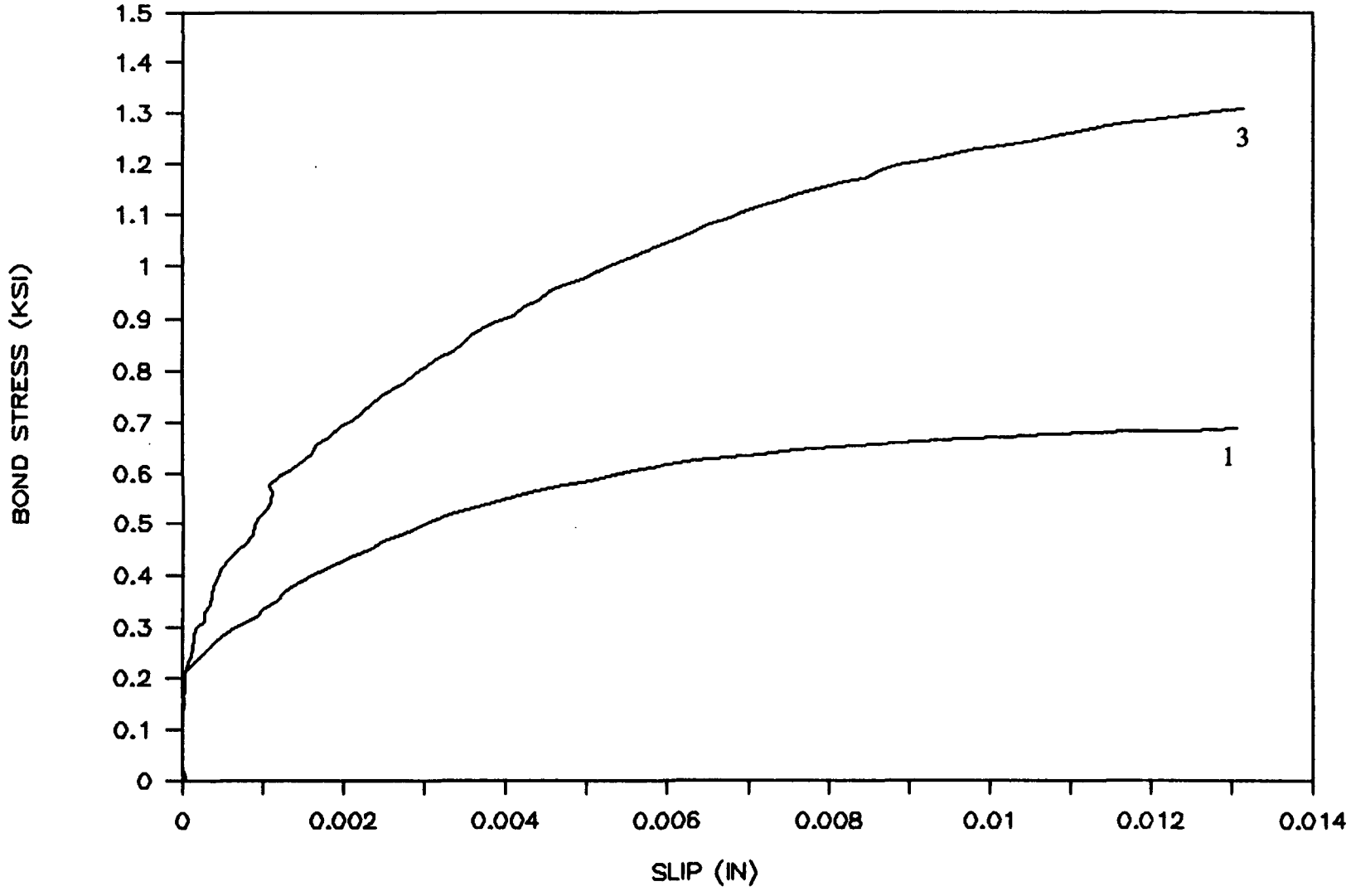

Figure 9a
Initial bond stress-slip curves: type A.

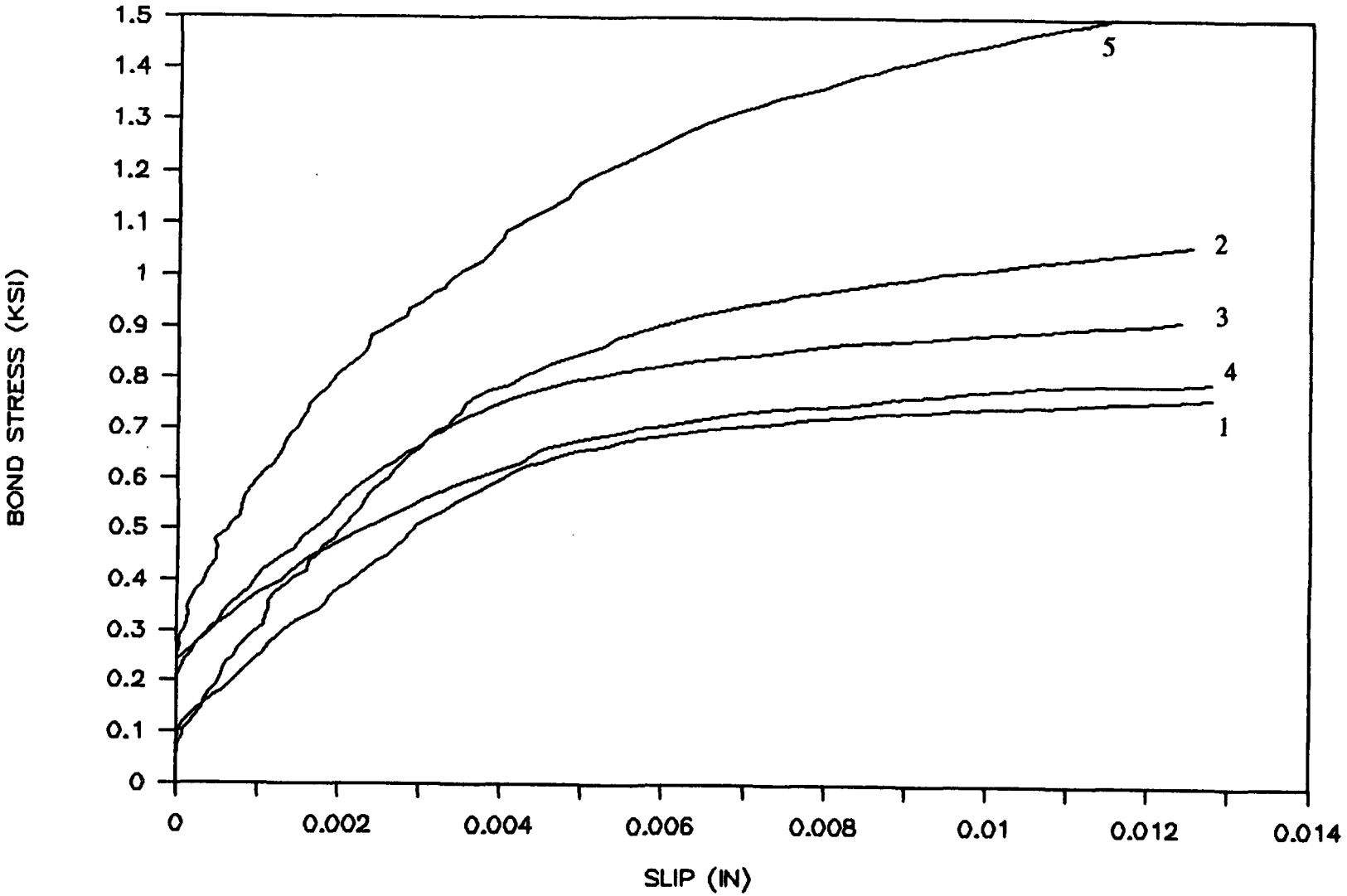

Figure 9b
Initial bond stress-slip curves: type B.

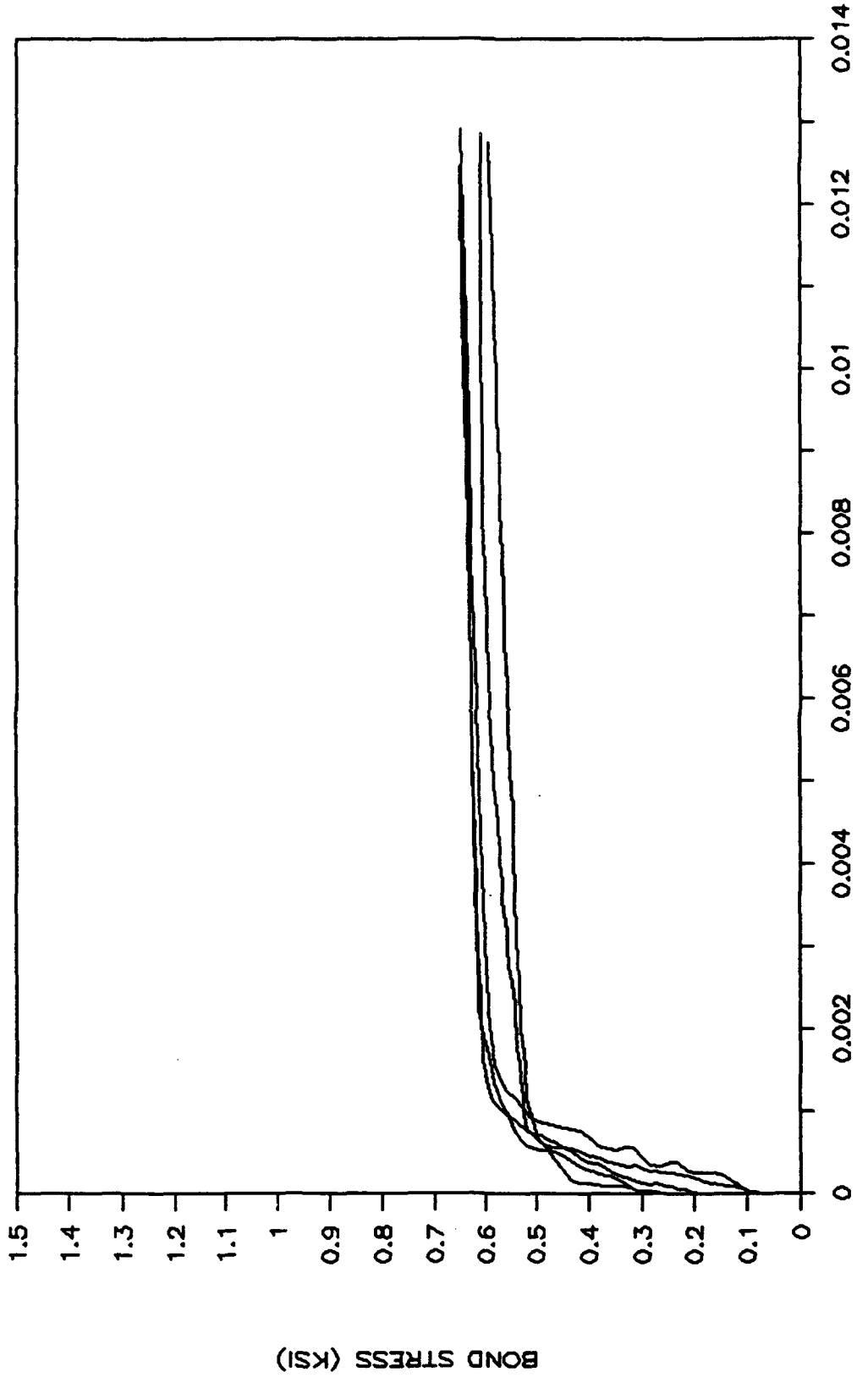

Figure 9c
Initial bond stress-slip curves: type C.

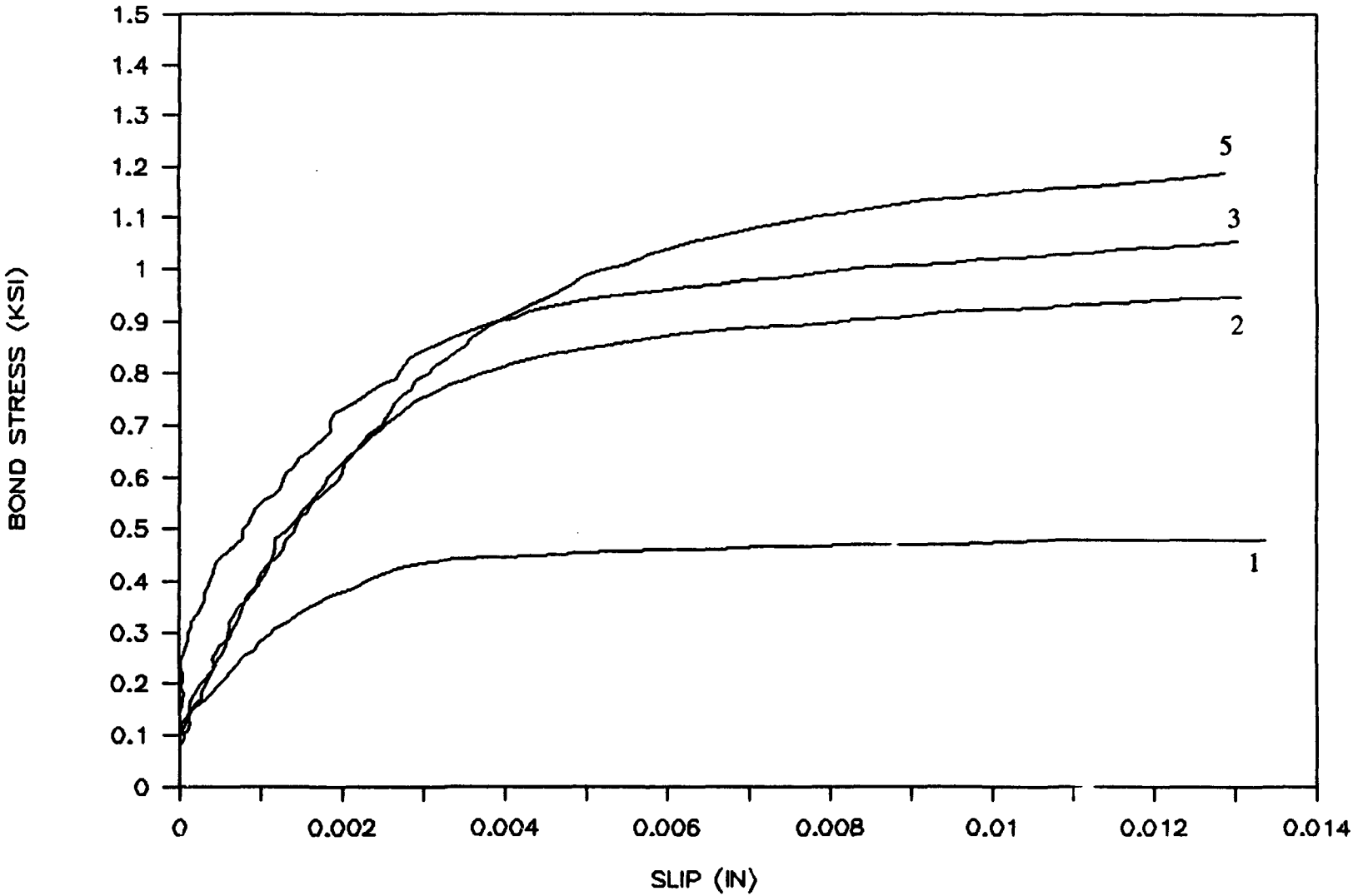

Figure 9d
Initial bond stress-slip curves: type D.

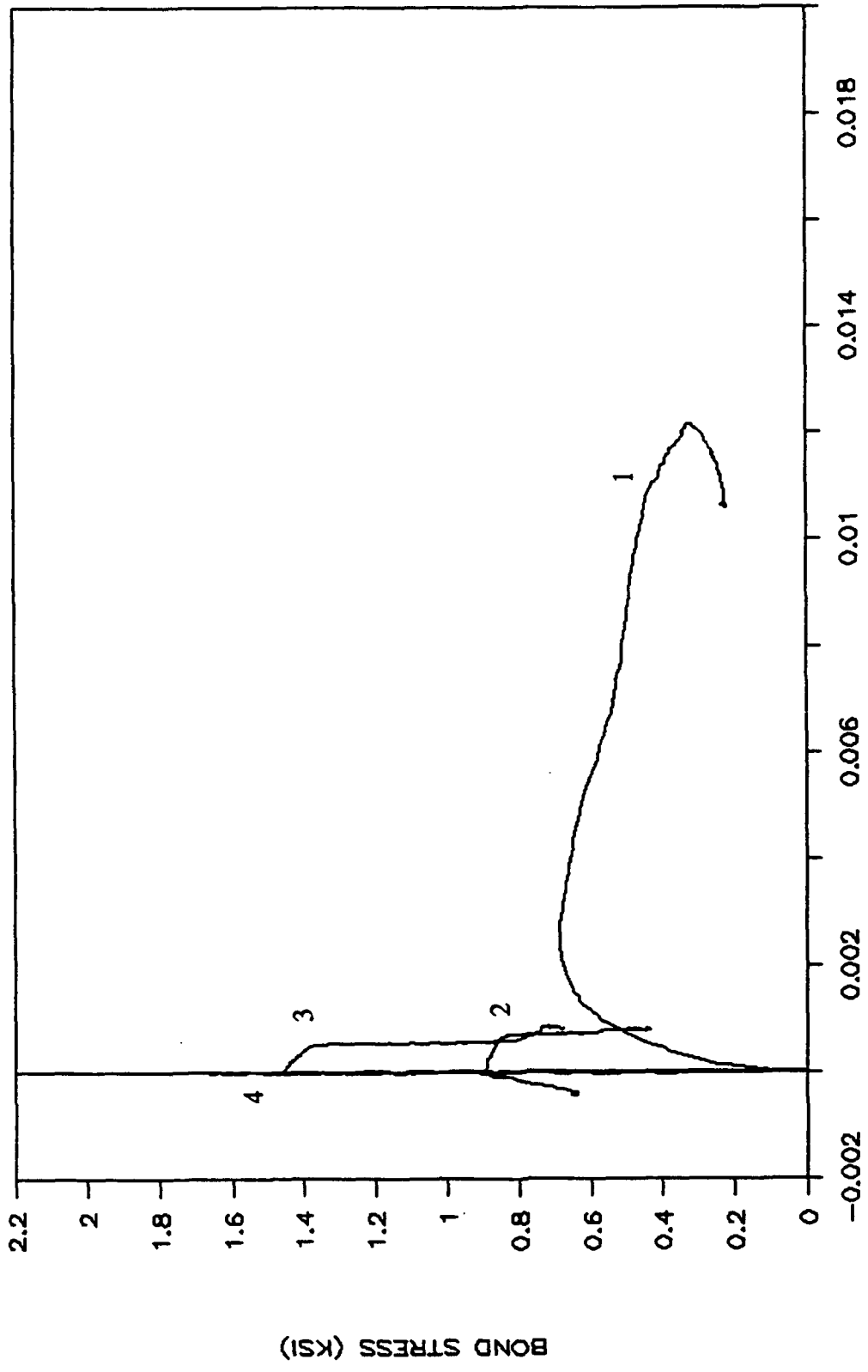

Figure 10a
Bond stress-radial displacement curves: type A.

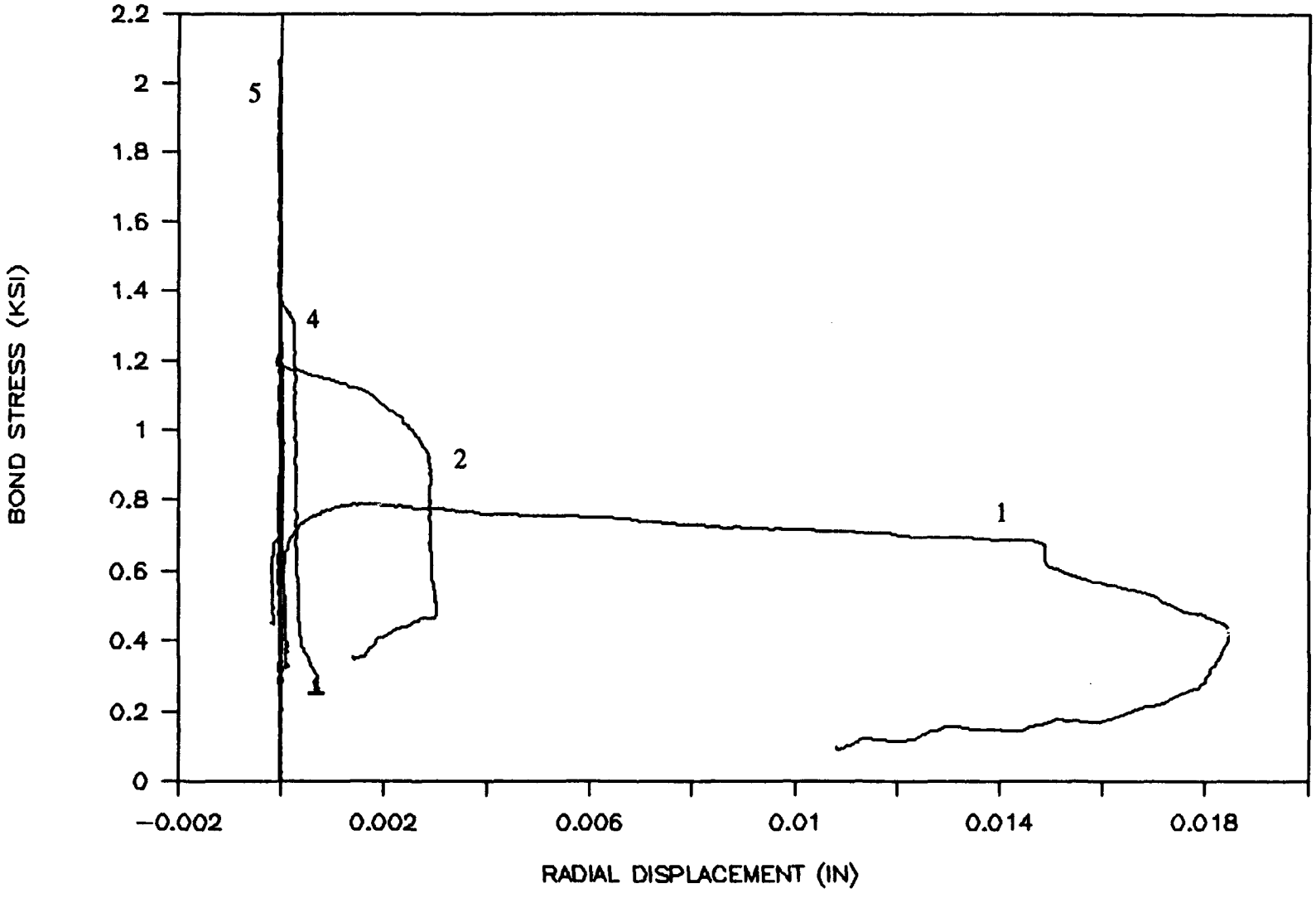

Figure 10b
Bond stress-radial displacement curves: type B.

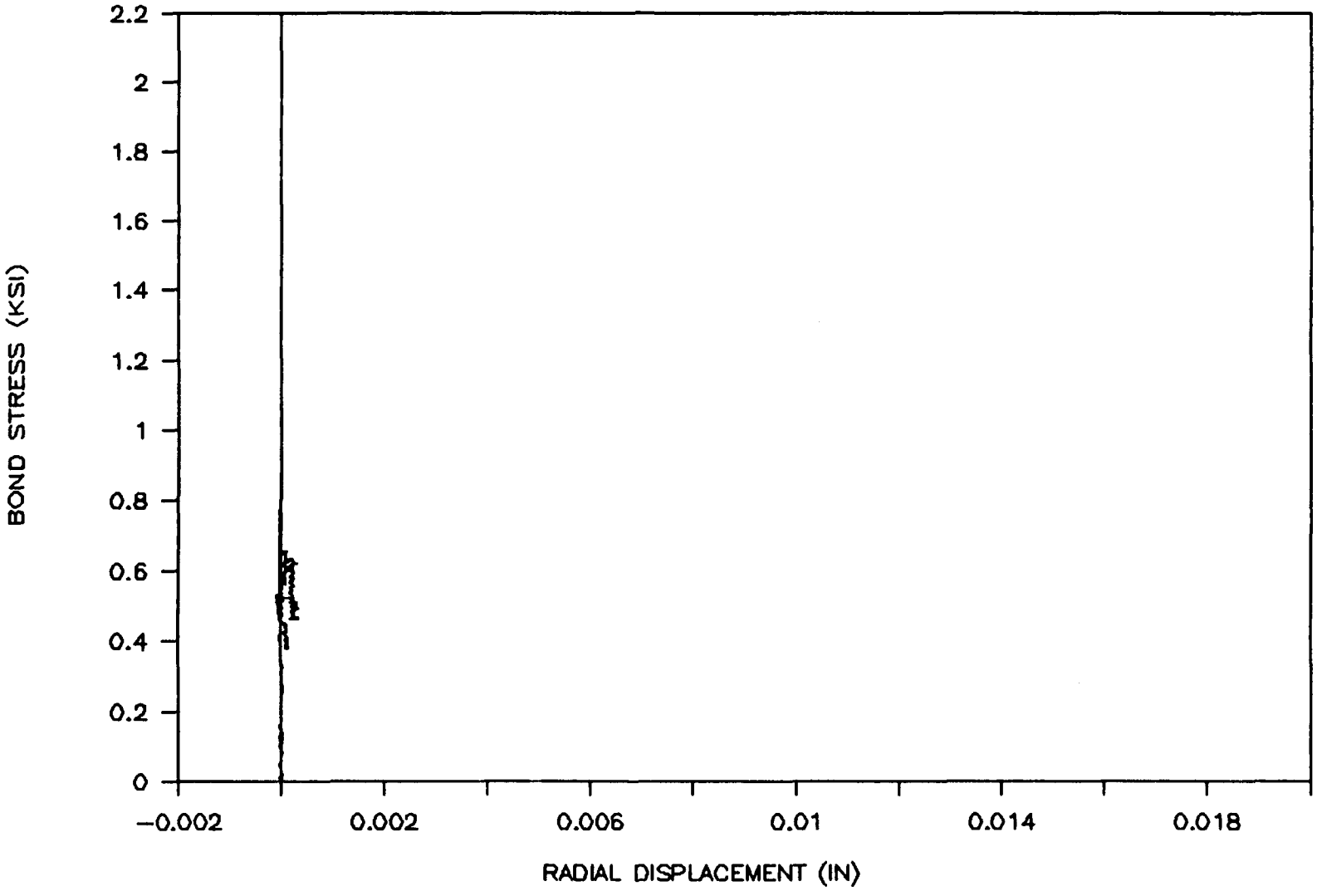

Figure 10c
Bond stress-radial displacement curves: type C.

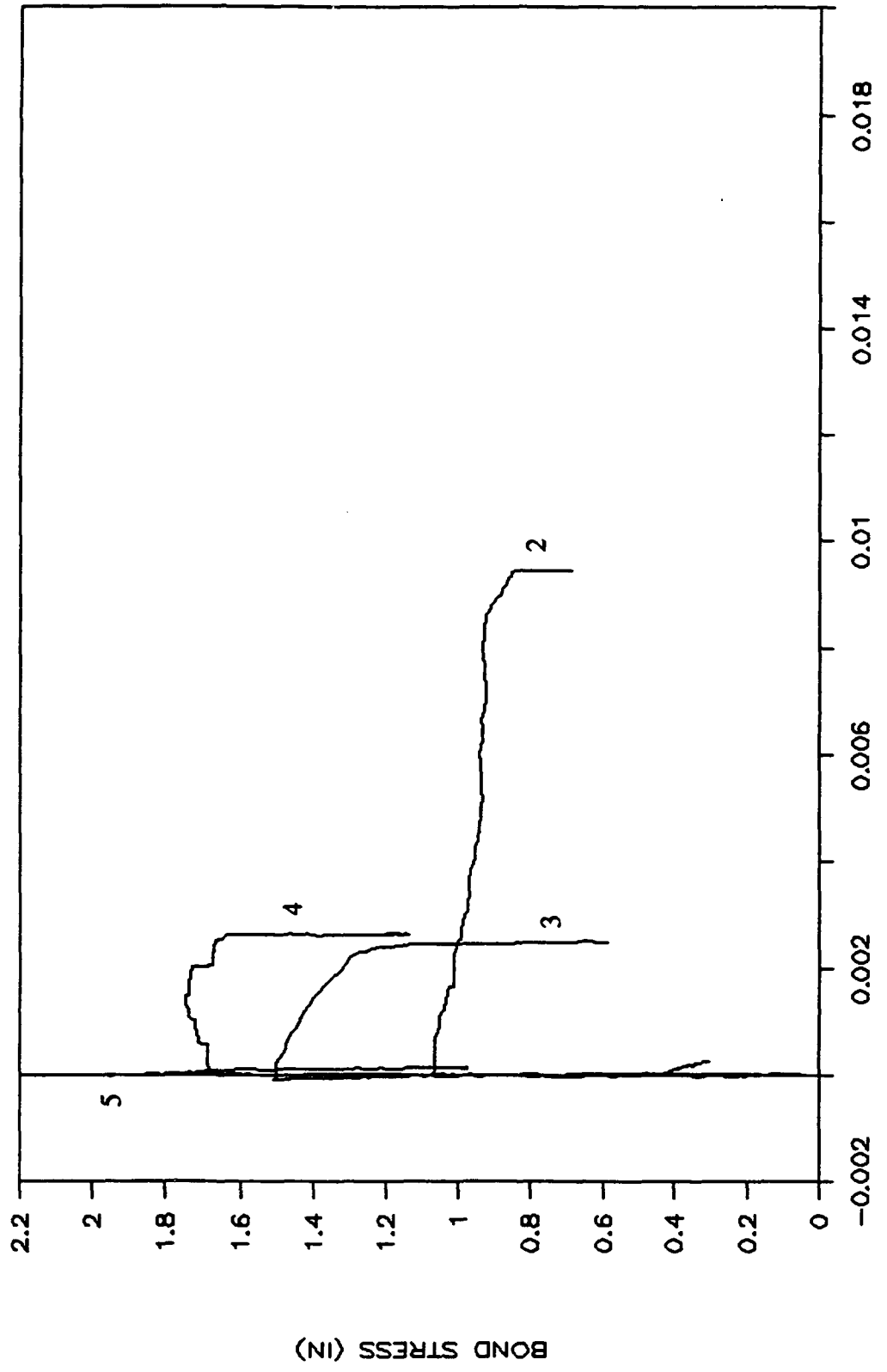

Figure 10d
Bond stress-radial displacement curves: type D.

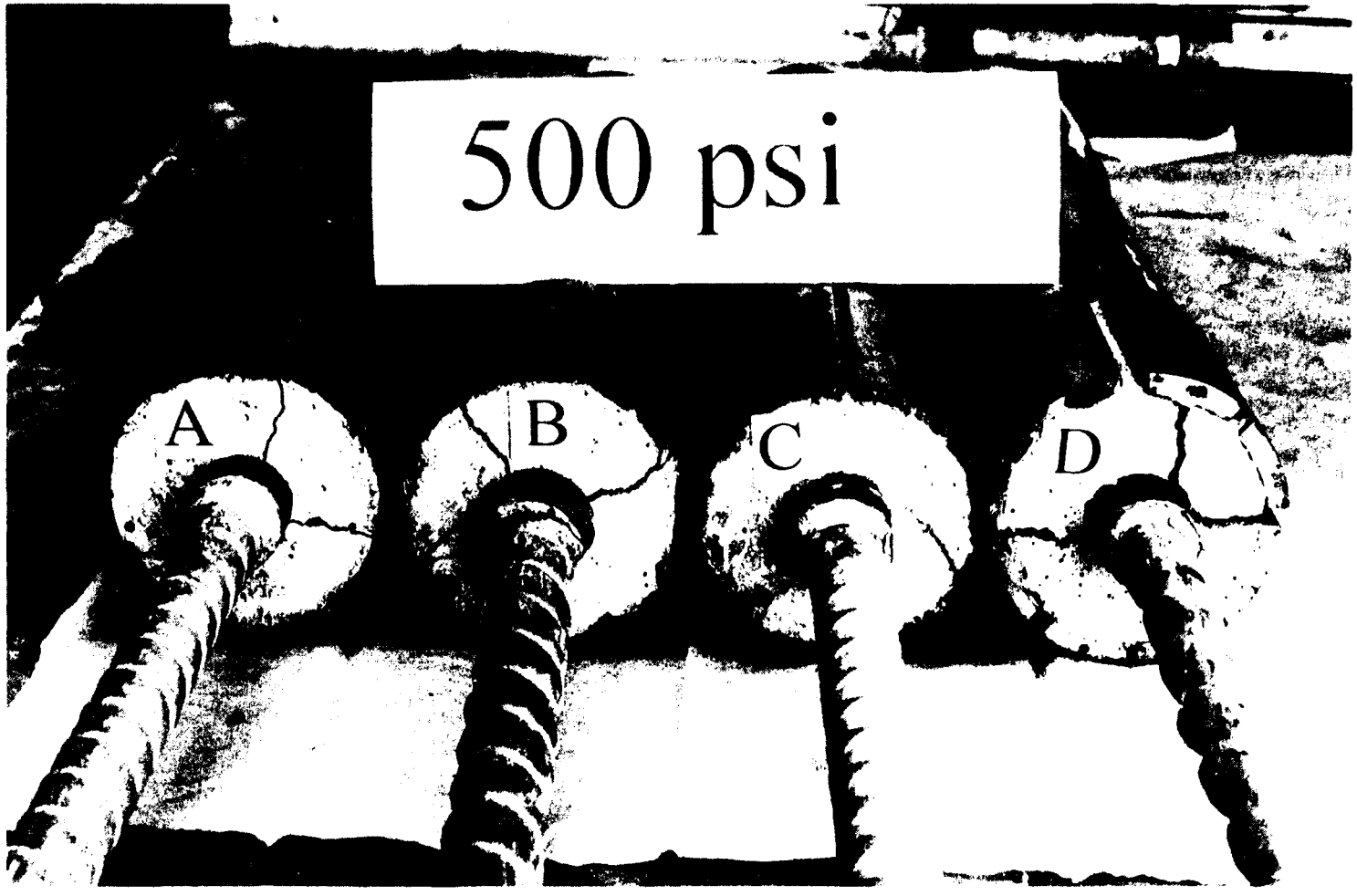

Figure 11a
Longitudinal cracks at low confining pressure.

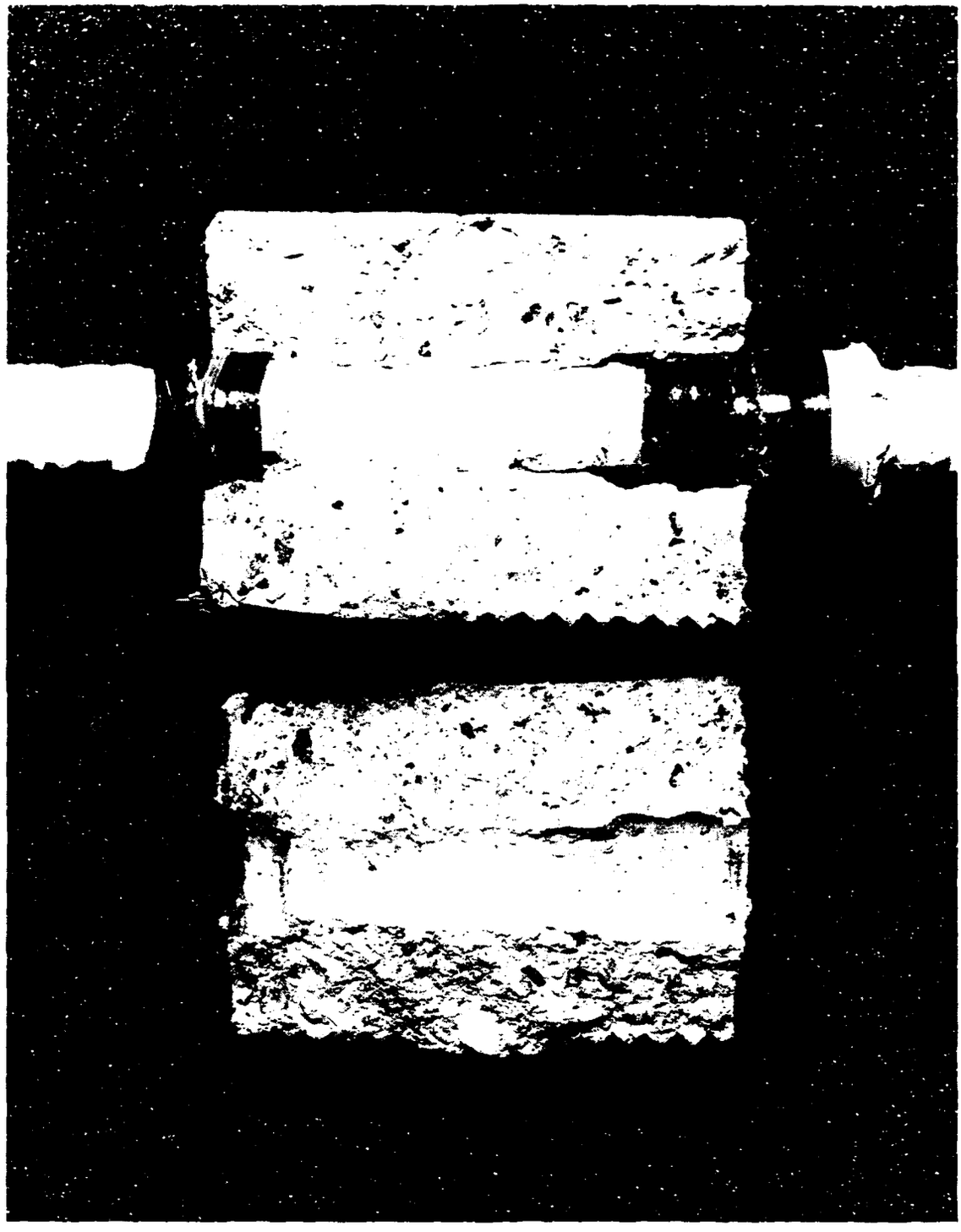

Figure 11b
Type A interface.

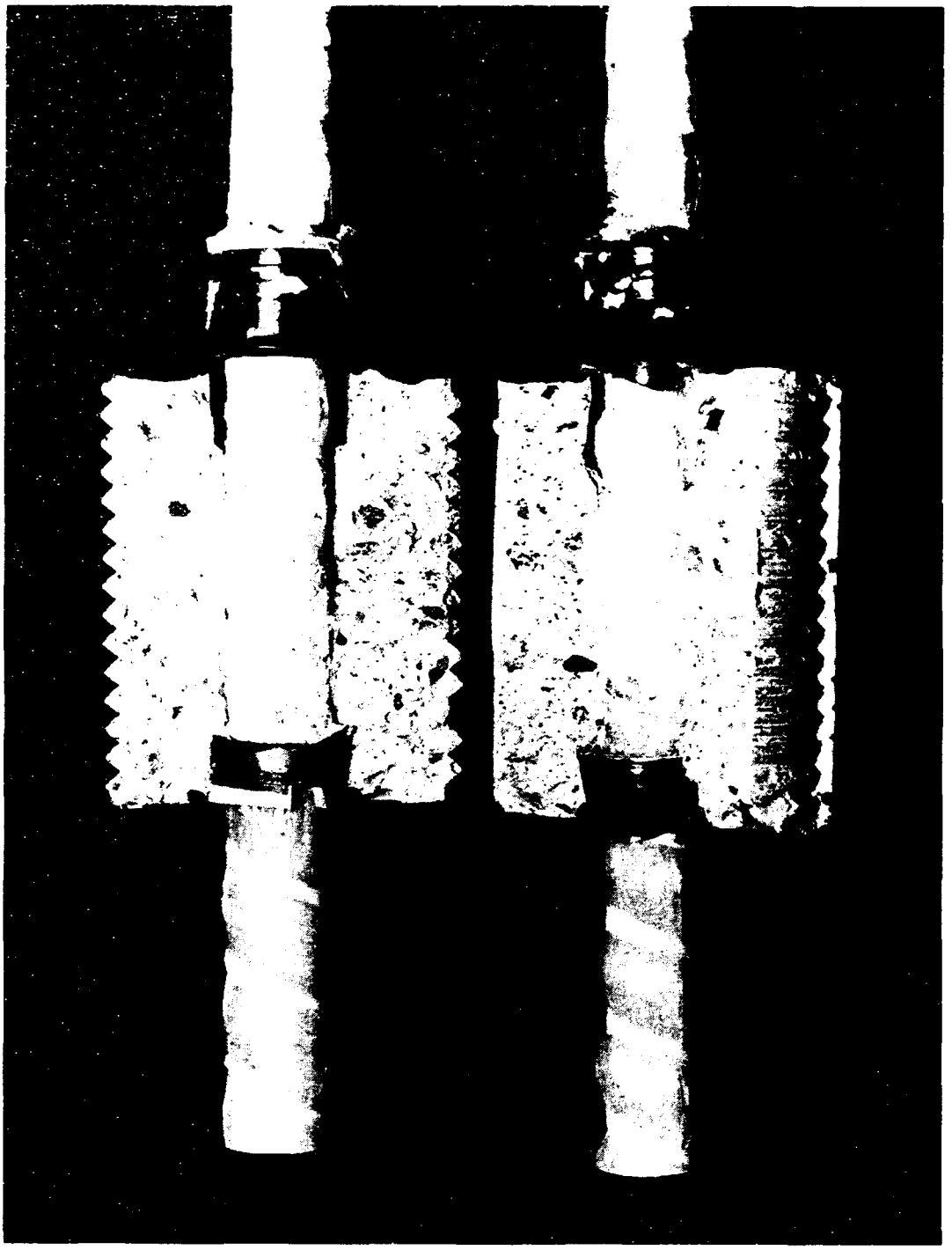

Figure 11c
Type B interface.

Figure 11d
Type C interface.

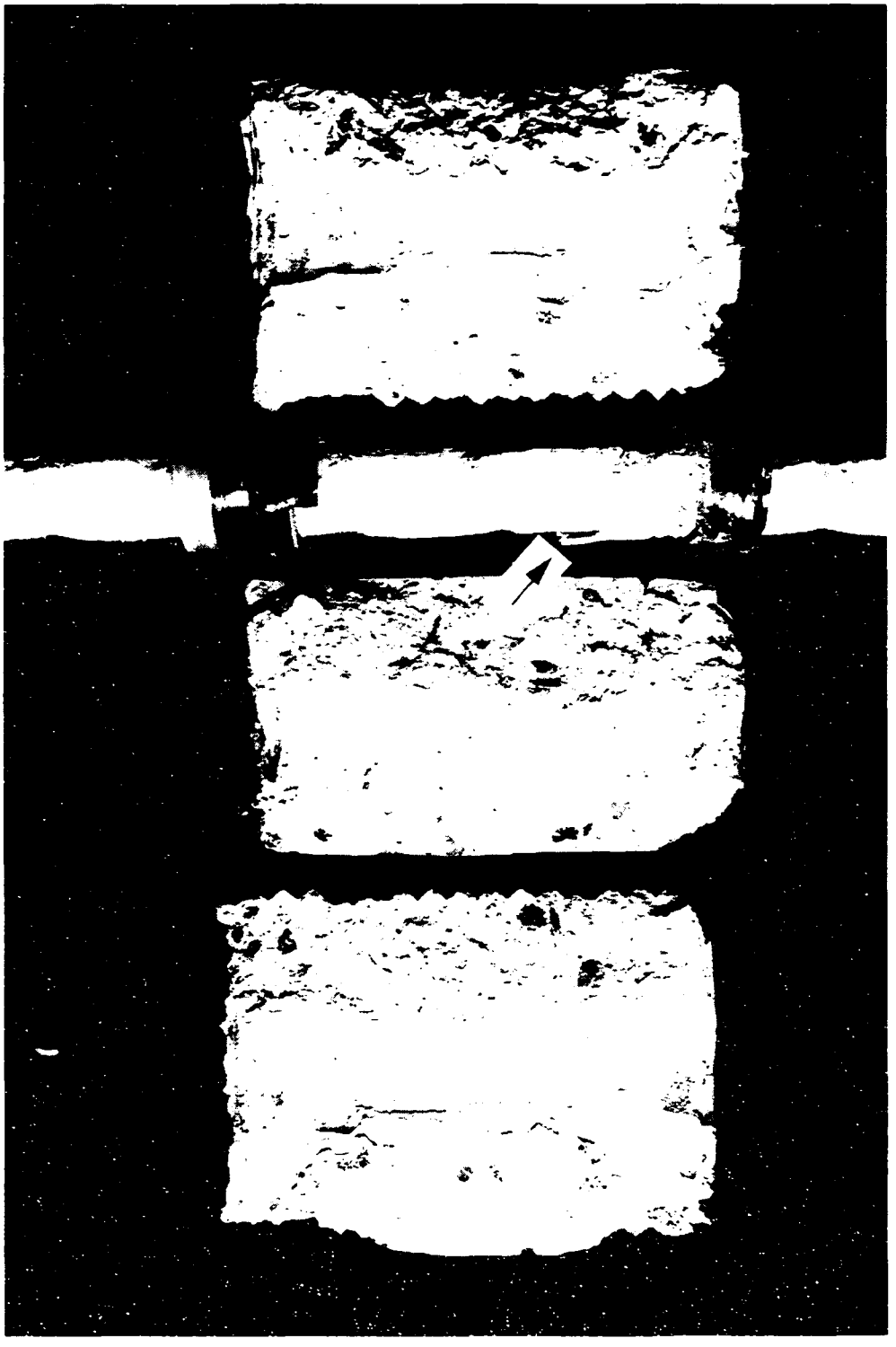

Figure 11e
Type D interface.

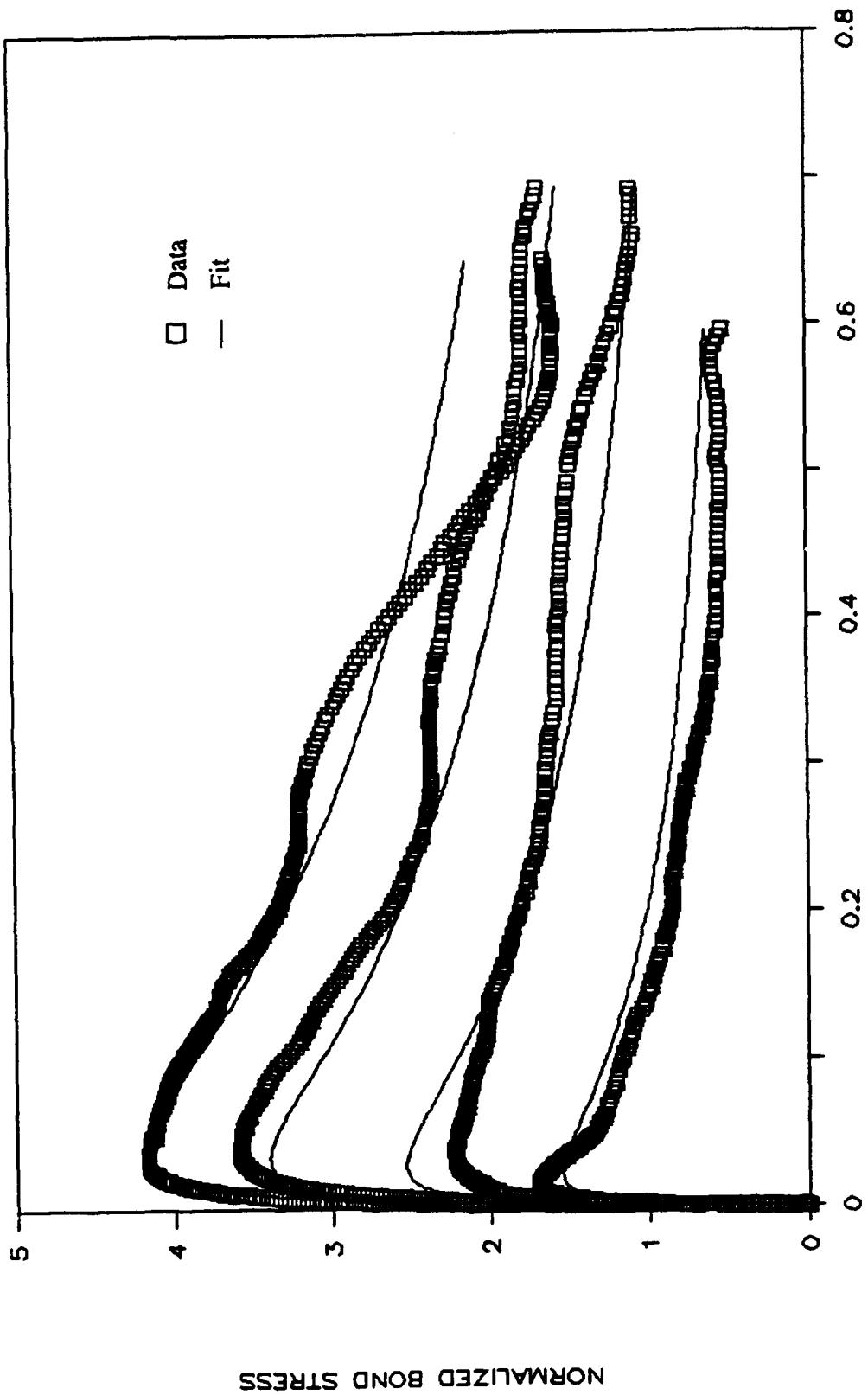

Figure 12a
Type A: Data fit.

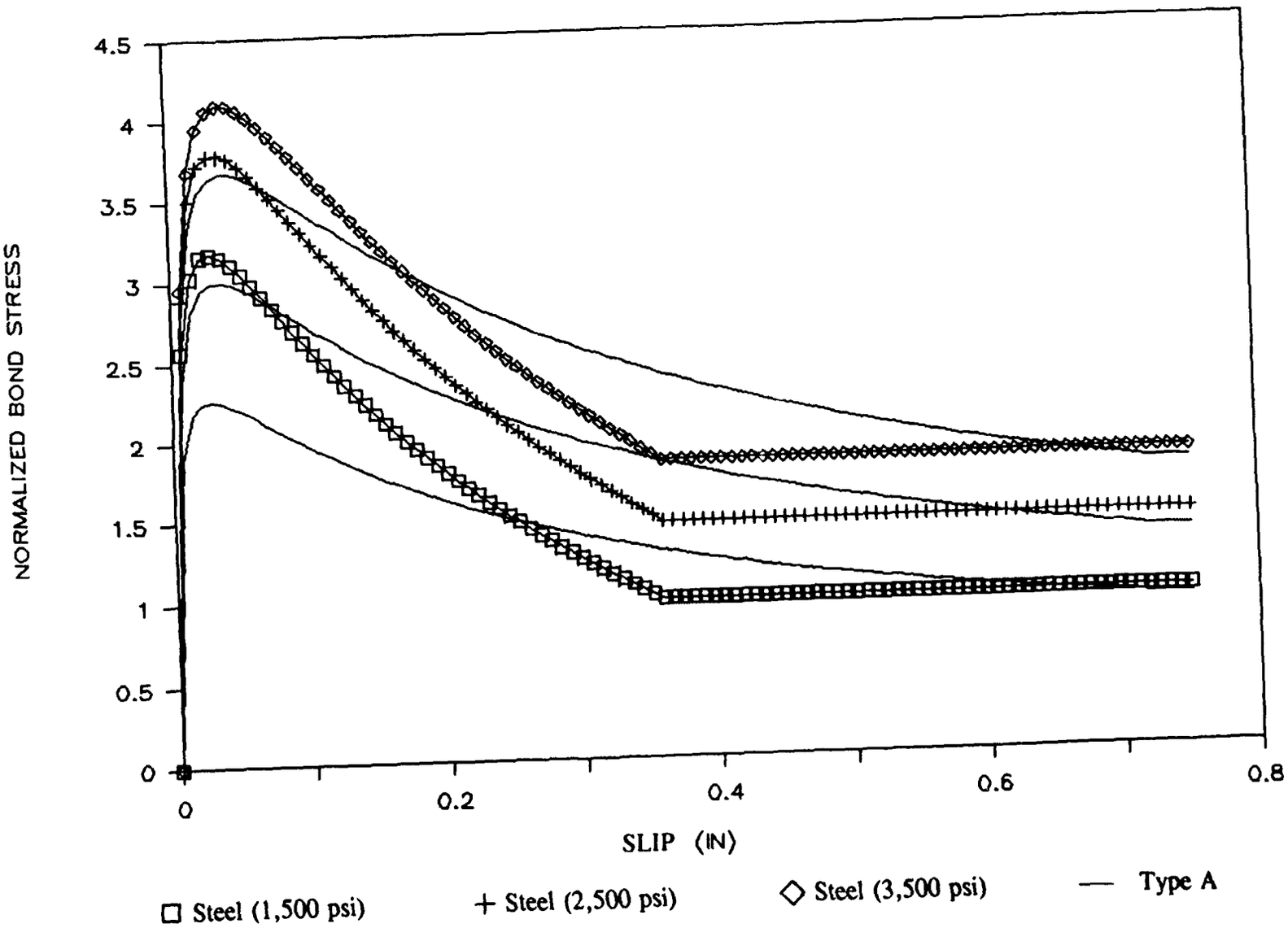

Figure 12b
Type A: Versus steel 68.

DISTRIBUTION LIST

ADINA ENGRG, INC / WALCZAK, WATERTOWN, MA
AFESC / TECH LIB, TYNDALL AFB, FL
AMERICAN CONCRETE / LIB, DETROIT, MI
ANATECH RESEARCH CORP / RASHID, SAN DIEGO, CA
APTEK / SCHWER, SAN JOSE, CA
ARMY CECOM R&D TECH LIBRARY / ASNC-ELC-I-T, FORT MONMOUTH, NJ
ARMY CERL / LIB, CHAMPAIGN, IL
ARMY ENGRG DIST / LIB, SEATTLE, WA
ARMY ENGRG DIST / LIB, PHILADELPHIA, PA
ARMY ENGRG DIST / LIB, PORTLAND, OR
BATTELLE NEW ENGLAND MARINE RSCH LAB / LIB, DUXBURY, MA
BECHTEL CIVIL, INC / K. MARK, SAN FRANCISCO, CA
BEN C GERWICK INC / FOTINOS, SAN FRANCISCO, CA
BETHLEHEM STEEL CO / ENGRG DEPT, BETHLEHEM, PA
CAL TECH / SCOTT, PASADENA, CA
CALTRANS / ZELINSKI, SACRAMENTO, CA
CASE WESTERN RESERVE UNIV / CE DEPT (PERDIKARIS), CLEVELAND, OH
CENTRIC ENGINEERING SYSTEMS INC / TAYLOR, PALO ALTO, CA
CHALMERS UNIVERSITY OF TECH / TEPFERS, SWEDEN,
CLARKSON UNIV / CEE DEPT, POTSDAM, NY
COLLEGE OF ENGINEERING / CE DEPT (AKINMUSURU), SOUTHFIELD, MI
COLLEGE OF ENGINEERING / CE DEPT (GRACE), SOUTHFIELD, MI
COLORADO SCHOOL OF MINES / DEPT OF ENGRG (CHUNG), GOLDEN, CO
CORNELL UNIV / CIVIL & ENVIRON ENGRG, ITHACA, NY
CORNELL UNIV / LIB, ITHACA, NY
CREATIVE PULTRUSIONS INC / SWEET, ALUM BANK, PA
DELFT UNIVERSITY OF TECH / DE BORST, GA DELFT, THE NETHERLANDS
DTIC / ALEXANDRIA, VA
ELICES, MANUEL / MADRID, SPAIN
FIBERGLAS / GREENWOOD, GRANVILL, OH
FLORIDA INST OF TECH / CE DEPT (KALAJIAN), MELBOURNE, FL
GEOCISA / RODRIGUEZ, COSLADA MADRID, SPAIN
GEORGE WASHINGTON UNIV / ENGRG & APP SCI SCHL (FOX), WASHINGTON, DC
GEORGIA INST OF TECH / CE SCHL (KAHN), ATLANTA, GA
GEORGIA INST OF TECH / CE SCHL (SWANGER), ATLANTA, GA
GEORGIA INST OF TECH / DR. J. DAVID FROST, ATLANTA, GA
GEORGIA TECH / CHAMEAU, ATLANTA, GA
GERWICK, BEN / SAN FRANCISCO, CA
HAN-PADRON ASSOCIATES / DENNIS PADRON, NEW YORK, NY
HAYNES & ASSOC / H. HAYNES, PE, OAKLAND, CA
HERCULES INC / COURTNEY, WILMINGTON, DE
HJ DEGENKOLB ASSOC / W. MURDOUGH, SAN FRANCISCO, CA
HKS INC / JOOP NAGTEGAAL, PROVIDENCE, RI
HUS INC / NAGTEGAAL, PAWTUCKET, RI
IMCO REINFORCED PLASTICS INC / LAMONICA, MOORESTOWN, NJ
JOHN HOPKINS UNIV / CE DEPT, JONES, BALTIMORE, MD
KARAGOZIAN & CASE STRUCTURAL ENGRS / CRAWFORD, GLENDALE, CA
LABORATOIRE CENTRAL DES PONTS ET CHAUSSEES / ROSSI, PARIS CEDEX 15, FRANCE
LABORATOIRE DE MECANIQUE ET TECHNOLOGIE / BERTHAUD, CACHAN, FRANCE
LAWRENCE LIVERMORE NATIONAL LAB / WHIRLEY LIVERMORE, CA
MARINE CONCRETE STRUCTURES, INC / W.A. INGRAHAM, METAIRIE, LA
MICHIGAN TECH UNIV / CO DEPT (HAAS), HOUGHTON, MI
NAVCOASTSYSCEN / CODE 423, PANAMA CITY, FL

NAVFACENGCOM / CODE 04B2 (J. CECILIO), ALEXANDRIA, VA
NBS / BLDG MAT DIV, MATHEY, GAITHERSBURG, MD
NEPTCO / RACZELOWSKI, PAWTUCKET, RI
NEW ZEALAND CONCRETE RSCH ASSN / LIB, PORIRUA,
NORTHWESTERN UNIVERSITY / BAZANT, EVANSTON, IL
NSF / STRUC & BLDG SYSTEMS (KP CHONG), WASHINGTON, DC
OCNR / CODE 10P4 (KOSTOFF), ARLINGTON, VA
OCNR / CODE 1121 (EA SILVA), ARLINGTON, VA
OCNR / CODE 1132SM, ARLINGTON, VA
OHIO STATE UNIVERSITY / CE DEPT (SIERAKOWSKY), COLUMBUS, OH
OREGON STATE UNIV / CE DEPT (HICKS), CORVALLIS, OR
PURDUE UNIV / CE SCOL (CHEN), WEST LAFAYETTE, IN
PURDUE UNIV / CE SCOL (RAMIREZ), WEST LAFAYETTE, IN
PWC / CODE 123C, SAN DIEGO, CA
REICHHOLD CHEMICALS INC / MCCLASKEY, RESEARCH TRIANGLE PARK, NC
SD SCHOOL OF MINES AND TECH / IYER, RAPID CITY, SD
SPI / BARNO, GRANVILLE, OH
STANFORD UNIV / DIV OF APPLIED MECHANICS, STANFORD, CA
TUFTS UNIV / SANAYEI, MEDFORD, MA
UCSD / SEIBLE, LA JOLLA, CA
UNIV OF ARIZONA / EHSANI, TUCSON, AZ
UNIV OF CALIFORNIA / CE DEPT (FOURNEY), LOS ANGELES, CA
UNIV OF CALIFORNIA / CE DEPT (HERRMANN), DAVIS, CA
UNIV OF CALIFORNIA / CE DEPT (RAMEY), DAVIS, CA
UNIV OF CALIFORNIA / CE DEPT (ROMSTADT), DAVIS, CA
UNIV OF CALIFORNIA / CE DEPT (SELNA), LOS ANGELES, CA
UNIV OF CALIFORNIA / CE DEPT (WILLIAMSON), BERKELEY, CA
UNIV OF CALIFORNIA / MECH ENGR (BAYO), SANTA BARBARA, CA
UNIV OF CALIFORNIA / MECH ENGR (MCMEEKING), SANTA BARBARA, CA
UNIV OF CALIFORNIA / MECH ENGRG DEPT (KEDWARD), SANTA BARBARA, CA
UNIV OF CALIFORNIA / MECH ENGRG DEPT (LECKIE), SANTA BARBARA, CA
UNIV OF COLORADO / MECH ENGRG DEPT (FELLIPA), BOULDER, CO
UNIV OF COLORADO / MECH ENGRG DEPT (WILLAM), BOULDER, CO
UNIV OF COLORADO / STURE, BOULDER, CO
UNIV OF HAWAII / MANOA, LIB, HONOLULU, HI
UNIV OF ILLINOIS / CE LAB (ABRAMS), URBANA, IL
UNIV OF ILLINOIS / CE LAB (PECKNOLD), URBANA, IL
UNIV OF ILLINOIS / METZ REF RM, URBANA, IL
UNIV OF MARYLAND / CE DEPT, COLLEGE PARK, MD
UNIV OF MICHIGAN / CE DEPT (RICHART), ANN ARBOR, MI
UNIV OF N CAROLINA / CE DEPT (GUPTA), RALEIGH, NC
UNIV OF NEW MEXICO / NMERI, HL SCHREYER, ALBUQUERQUE, NM
UNIV OF RHODE ISLAND / CE DEPT (LEE), KINGSTON, RI
UNIV OF TEXAS / CONSTRUCTION INDUSTRY INST, AUSTIN, TX
UNIV OF TEXAS / ECJ 5.402 (TUCKER), AUSTIN, TX
UNIV OF TEXAS / ROESSET, AUSTIN, TX
UNIV OF WASHINGTON / CE DEPT (MATTOCK), SEATTLE, WA
UNIV OF WYOMING / CE DEPT, LARAMIE, WY
UNIV OF WYOMING / SCHMIDT, LARAMIE, WY
USCOE / LAMPO, CHAMPAIGN, IL
WEIDLINGER ASSOC / F.S. WONG, LOS ALTOS, CA
WISS, JANNEY, ELSTNER, & ASSOC / DW PFEIFER, NORTHBROOK, IL